

Analysis strategies for general spin-independent WIMP-nucleus scatteringMartin Hoferichter,^{1,*} Philipp Klos,^{2,3,†} Javier Menéndez,^{4,‡} and Achim Schwenk^{2,3,5,§}¹*Institute for Nuclear Theory, University of Washington, Seattle, Washington 98195-1550, USA*²*Institut für Kernphysik, Technische Universität Darmstadt, 64289 Darmstadt, Germany*³*ExtreMe Matter Institute EMMI, GSI Helmholtzzentrum für Schwerionenforschung GmbH, 64291 Darmstadt, Germany*⁴*Department of Physics, The University of Tokyo, 113-0033 Tokyo, Japan*⁵*Max-Planck-Institut für Kernphysik, Saupfercheckweg 1, 69117 Heidelberg, Germany*

(Received 26 May 2016; published 8 September 2016)

We propose a formalism for the analysis of direct-detection dark-matter searches that covers all coherent responses for scalar and vector interactions and incorporates QCD constraints imposed by chiral symmetry, including all one- and two-body WIMP-nucleon interactions up to third order in chiral effective field theory. One of the free parameters in the WIMP-nucleus cross section corresponds to standard spin-independent searches, but in general different combinations of new-physics couplings are probed. We identify the interference with the isovector counterpart of the standard spin-independent response and two-body currents as the dominant corrections to the leading spin-independent structure factor, and discuss the general consequences for the interpretation of direct-detection experiments, including minimal extensions of the standard spin-independent analysis. Fits for all structure factors required for the scattering off xenon targets are provided based on state-of-the-art nuclear shell-model calculations.

DOI: [10.1103/PhysRevD.94.063505](https://doi.org/10.1103/PhysRevD.94.063505)**I. INTRODUCTION**

Direct searches for the nuclear recoil produced by weakly interacting massive particles (WIMPs) on target nuclei in large-scale detectors provide a prime avenue to unravel the nature of dark matter, complementary to indirect searches for annihilation remnants in astrophysical observations and the production of dark-matter particles in collider experiments [1]. However, for the interpretation of current experimental limits, e.g. [2–10], it is crucial that the nuclear aspects of direct-detection experiments be adequately addressed. This is especially important given the impressive experimental efforts that include future liquid-noble-gas ton-scale experiments already in commissioning such as XENON1T [11], DEAP-3600 [12], and ArDM [13], or in planning phase, LZ [14], XENONnT [15], XMASS [16], DarkSide-20k [17], and DARWIN [18]; but also smaller-scale experiments such as SuperCDMS SNOLAB [19], DAMIC100 [20], or CRESST [21] that focus on light WIMPs with masses below 10 GeV.

Standard analyses of WIMP-nucleus scattering are formulated in terms of spin-independent (SI) and spin-dependent (SD) searches [22], named after the nature of the WIMP-nucleon interactions at low energies. At the same time, SI and SD scattering are characterized by a very different scaling of the corresponding structure factors: while for SI scattering the response is proportional to the total number of nucleons A^2 , the scale of SD scattering is set by the spin expectation value of

the unpaired nucleon. Due to the coherent enhancement of SI interactions, the corresponding limits on the WIMP-nucleon couplings set by direct-detection experiments are orders of magnitude more stringent than for SD searches, but each type of interaction is sensitive to different operators for the coupling of WIMPs with Standard-Model fields. For instance, while quark-WIMP scalar-scalar and vector-vector terms contribute to the SI response, the SD interaction is generated by axial-vector–axial-vector operators. Additional information on the WIMP nature can be extracted from inelastic scattering off the target nuclei [23,24].

Corrections to standard SI and SD responses are conveniently studied in terms of effective field theories (EFTs). In this context, the calculation of nuclear structure factors has been organized in two different ways: first, non-relativistic EFT (NREFT) for nucleon and WIMP fields [25–28] allows a study of the nuclear responses as a function of the effective couplings in the EFT, and to extract limits on the coefficients of the NREFT operators [29]. Second, in order to translate the NREFT limits to the parameter space of a given new-physics model, the QCD dynamics integrated out in the NREFT approach needs to be included. Particularly important are the consequences of the spontaneous breaking of the chiral symmetry of QCD, which can be explored within the framework of chiral EFT (ChEFT), see Refs. [30–33] for recent reviews. The analysis within ChEFT establishes relations between different NREFT operators, and provides a counting scheme that indicates at which order contributions beyond the single-nucleon level [34–37] need to be included. Recent work in this direction includes ChEFT-based structure factors for

* mhofer@uw.edu

† pklos@theorie.ikp.physik.tu-darmstadt.de

‡ menendez@nt.phys.s.u-tokyo.ac.jp

§ schwenk@physik.tu-darmstadt.de

the SD response [36,38], aspects of SI scattering [35,39,40], inelastic scattering [23], as well as a general ChEFT analysis of one- and two-body currents [37].

In the present work we provide a generalization of SI scattering that includes all coherent contributions up to third order in ChEFT [37]. This involves considering two-body currents, but also momentum corrections to the nucleon form factors predicted at the same ChEFT order. We provide a detailed discussion of the structure factor associated with the scalar two-body current studied before in the literature, and extend the analysis to include the two-body current generated by the coupling of the trace anomaly of the QCD energy-momentum tensor to the pion in flight, which becomes important if the WIMP couples (significantly) via gluonic interactions. In addition, an analysis of the NREFT operators reveals that in general there are six relevant nuclear operators, denoted by M , Σ' , Σ'' , Δ , $\tilde{\Phi}'$, and Φ'' [26,28], where M corresponds to the standard SI scattering, while a combination of Σ' and Σ'' yields the operator relevant for the SD case. Given that apart from M also Φ'' can be coherently enhanced (which is especially the case in heavy nuclei) and that M and Φ'' interfere, a generalization of the traditional SI analysis should also take the effects from Φ'' into account [26].

We note that for general SI scattering, new combinations of Wilson coefficients are probed by the two-body currents coupling to the exchanged pion in flight, and also by the corrections to the nucleon form factors and the contributions associated with the Φ'' operator. This is in contrast to the SD case, where the dominant two-body currents can be absorbed into a redefinition of the one-body structure factors, i.e., the two-body correction is sensitive to the same physics beyond the Standard Model (BSM) as the standard SD interaction [36,38]. In a similar way to the SI analysis presented here, a more general SD analysis should include the effects of all relevant nuclear operators and two-body currents.

This work is organized as follows. We start with an overview of the main results in Sec. II, where we propose an analysis strategy for direct-detection experiments that generalizes the standard SI case. The general formalism is detailed in Sec. III, where we lay out the decomposition of the WIMP-nucleus scattering rate, collect the relevant nucleon matrix elements, and introduce the Wilson coefficients that parametrize the WIMP-quark and WIMP-gluon interactions. We then formulate a set of generalized structure factors that includes effects from two-body currents, corrections to the nucleon form factors, and the nuclear Φ'' operator. In Sec. IV we present state-of-the-art nuclear shell-model calculations for the structure factors corresponding to one-body currents in all relevant xenon isotopes, before developing a generalization for the two-body currents in Sec. V. In Sec. VI we discuss the size of the nucleon form-factor corrections as well as the number of independent parameters in generalized SI scattering, and

work out in detail the size of the corrections to standard SI scattering for two simple models. We conclude with a short summary in Sec. VII. While our analysis strategy is general, the numerical results presented here are focused on WIMPs scattering off xenon nuclei, leaving the nuclear structure calculations for other targets to future work.

II. OVERVIEW OF MAIN RESULTS AND ANALYSIS STRATEGIES

Standard analyses of dark-matter direct-detection experiments distinguish between SI and SD scattering based on the nature of the WIMP-nucleon interaction. At the same time, these two cases generate very different nuclear responses, as SI scattering is enhanced by the coherent contribution of all nucleons in the nucleus, whereas the scale of SD scattering is set by a single-nucleon matrix element.

When subleading contributions in EFTs are considered, the classification of the different terms according to the nature of the WIMP-nucleon interaction becomes less useful, given that the coherent enhancement associated with the combined contribution of a significant number of nucleons is also common to NREFT operators that may involve a WIMP or even a nucleon spin operator. Such responses are closer in their experimental signature to the traditional SI interactions in the sense that the associated structure factors are enhanced compared to the single-nucleon case.

Therefore we propose to define generalized SI scattering not by the form of the NREFT operator, but based on whether a coherent enhancement is possible. In this spirit, a general decomposition of the WIMP-nucleus cross section $\sigma_{\chi N}^{\text{SI}}$ should include the coherently enhanced corrections generated by

- (1) the standard SI isoscalar WIMP-nucleon interaction,
- (2) its isovector counterpart,
- (3) the interaction of the WIMP with two nucleons via two-body (meson-exchange) currents,
- (4) momentum-dependent corrections to the nucleon form factors,
- (5) the quasicohherent response associated with the Φ'' operator (related to the nucleon spin-orbit operator).

The proposed generalization amounts to the decomposition of the WIMP-nucleus cross section

$$\begin{aligned} \frac{d\sigma_{\chi N}^{\text{SI}}}{d\mathbf{q}^2} = & \frac{1}{4\pi v^2} \left| \left(c_+^M - \frac{\mathbf{q}^2}{m_N^2} \dot{c}_+^M \right) \mathcal{F}_+^M(\mathbf{q}^2) + c_\pi \mathcal{F}_\pi(\mathbf{q}^2) \right. \\ & + c_\pi^\theta \mathcal{F}_\pi^\theta(\mathbf{q}^2) + \left(c_-^M - \frac{\mathbf{q}^2}{m_N^2} \dot{c}_-^M \right) \mathcal{F}_-^M(\mathbf{q}^2) \\ & \left. + \frac{\mathbf{q}^2}{2m_N^2} [c_+^{\Phi''} \mathcal{F}_+^{\Phi''}(\mathbf{q}^2) + c_-^{\Phi''} \mathcal{F}_-^{\Phi''}(\mathbf{q}^2)] \right|^2, \end{aligned} \quad (1)$$

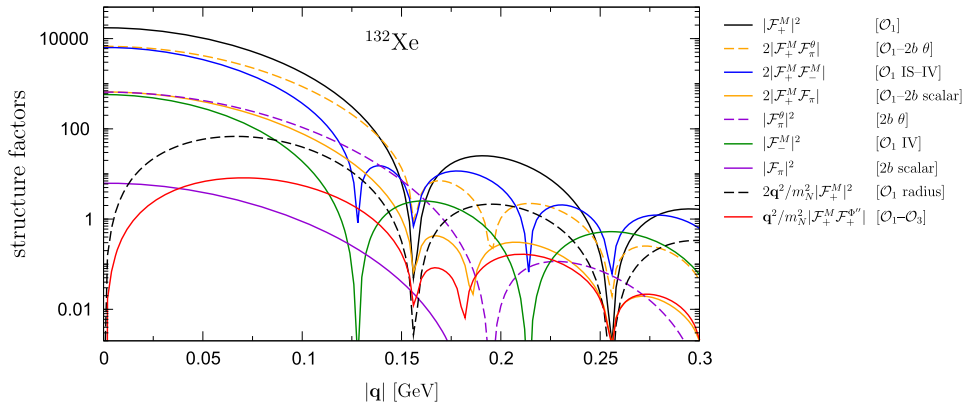


FIG. 1. Comparison of the leading structure factors associated with the coherent and quasicohherent one-body \mathcal{F}^M and $\mathcal{F}^{\Phi'}$ nuclear responses, the two-body nuclear responses \mathcal{F}_π (solid lines) and \mathcal{F}_π^θ (dashed lines), and the radius corrections (\hat{c}) to the structure factors. The individual contributions are ordered in the legend according to their size at $|\mathbf{q}| = 0$ (from top to bottom): the standard SI response \mathcal{F}_+^M corresponding to the isoscalar one-body \mathcal{O}_1 operator (black), its interference with an \mathcal{O}_1 isovector contribution (blue) and with the two-body responses \mathcal{F}_π and \mathcal{F}_π^θ (orange), the purely isovector contribution \mathcal{F}_-^M (green) and the structure factor generated solely by the two-body currents (violet), the momentum-dependent radius correction to \mathcal{O}_1 (black dashed), and the interference of the standard SI response with the quasicohherent one-body $\mathcal{F}^{\Phi'}$ structure factor (red). The results, representative for all stable xenon isotopes, are shown for the most abundant ^{132}Xe .

where \mathbf{q} is the momentum transfer, \mathbf{v} the WIMP velocity, and, generically, the nuclear responses are denoted by \mathcal{F} and the free parameters that include BSM physics by c . This cross section includes all coherent contributions mentioned above and all terms up to third order in ChEFT [37]. First, the standard SI nuclear \mathcal{F}^M response, associated with the NREFT operator \mathcal{O}_1 [see Eq. (35) for definitions of the NREFT \mathcal{O}_i operators], can be sensitive to protons and neutrons in the same way (isoscalar, +), as considered in standard SI analyses, but also in the opposite way (isovector, -). Given that the heavy nuclei typically used for direct-detection experiments have a substantial neutron excess, the resulting isovector structure factor is coherently enhanced as well. Next, the power counting of ChEFT predicts to this order two-body interactions (parametrized by the nuclear \mathcal{F}_π and \mathcal{F}_π^θ responses for the coupling to the pion via a scalar current and via the trace anomaly of the QCD energy-momentum tensor θ_μ^μ , respectively) and momentum-dependent corrections to \mathcal{O}_1 (represented by \hat{c}), both of which are coherent. Finally, contributions from subleading NREFT operators can also be significantly coherent, the most relevant being \mathcal{O}_3 , which is related to the nucleon spin-orbit operator and gives rise to the nuclear $\mathcal{F}^{\Phi'}$ response. Here the coherence is also found in both isoscalar and isovector cases.

Equation (1) reflects the different particle, hadronic, and nuclear scales involved in WIMP-nucleus scattering. Within a given new-physics model, WIMPs interact with quark and gluon degrees of freedom, which are then to be embedded into the nucleon sector. In an EFT approach the BSM interaction is encoded in the Wilson coefficients of effective operators, while the nucleon matrix elements are

decomposed into nucleon form factors. As a result, the free coefficients c_\pm^M , c_π , c_π^θ , \hat{c}_\pm^M , and $\hat{c}_\pm^{\Phi'}$ correspond to a convolution of Wilson coefficients and nucleon matrix elements. In a final step, the nuclear responses \mathcal{F}_\pm^M , \mathcal{F}_π , \mathcal{F}_π^θ , and $\mathcal{F}^{\Phi'}$ take into account that the scattering occurs in the nucleus, a strongly interacting many-nucleon system. In this work, the relation between the free parameters c_\pm^M , c_π , c_π^θ , \hat{c}_\pm^M , $\hat{c}_\pm^{\Phi'}$ and the BSM Wilson coefficients is worked out in Sec. III for the case of a spin-1/2 WIMP, see also Eqs. (59)–(62) for the explicit relations. The nuclear responses \mathcal{F}_\pm^M , \mathcal{F}_π , \mathcal{F}_π^θ , and $\mathcal{F}^{\Phi'}$ are calculated in the framework of the nuclear shell model, with fit functions given for all stable xenon isotopes in Sec. IV for one-body currents and in Sec. V for two-body currents.

The size of the individual terms in Eq. (1) depends on a given new-physics model, which, together with the nucleon matrix elements, fixes the coefficients c . Nevertheless the nuclear responses \mathcal{F} already imply a strong hierarchy by themselves. This is illustrated in Fig. 1, where the different structure factors including interference terms are compared under the assumption that all coefficients are the same. As expected, the dominant correction originates from the interference of isoscalar and isovector \mathcal{F}_\pm^M responses. Next in the hierarchy is the interference with the two-body responses \mathcal{F}_π and \mathcal{F}_π^θ . The additional corrections included in Fig. 1 (apart from the pure isovector \mathcal{F}_- and pure two-body contributions) vanish at $|\mathbf{q}| = 0$, and are therefore suppressed at small \mathbf{q} compared to \mathcal{O}_1 and the two-body structure factors. We have also considered further higher-order NREFT one-body operators, but their contribution is even more suppressed, see Secs. III D and IV. Let us emphasize again that the hierarchy of the structure factors

in Fig. 1 assumes a common value for the c coefficients, but these are not in general independent and relative suppressions or enhancements may occur. In Sec. VIC we study the relative size of the isovector and two-body contributions in two simple models, which for instance suggests that the large \mathcal{F}_π^θ structure factor tends to be compensated by a large single-nucleon matrix element, leading to a relative two-body effect similar to that of the \mathcal{F}_π contribution.

Despite the potential impact of the c coefficients on the measured rate, the hierarchy of the nuclear structure factors observed in Fig. 1 is sufficiently pronounced to motivate a minimal extension of the standard SI scattering of the form

$$\frac{d\sigma_{\chi\mathcal{N}}^{\text{SI}}}{d\mathbf{q}^2} = \frac{1}{4\pi\mathbf{v}^2} \left| c_+^M \mathcal{F}_+^M(\mathbf{q}^2) + c_-^M \mathcal{F}_-^M(\mathbf{q}^2) + c_\pi \mathcal{F}_\pi(\mathbf{q}^2) + c_\pi^\theta \mathcal{F}_\pi^\theta(\mathbf{q}^2) \right|^2, \quad (2)$$

with only four independent parameters.

Since the nuclear responses can be obtained from nuclear-structure calculations, direct-detection experiments provide constraints on the c parameters. Although as discussed above, the limits on the direct-detection rate constrain additional combinations of Wilson coefficients and nucleon matrix elements, so far standard SI analyses have only considered the coefficient c_+^M , which is then related to the WIMP-nucleon cross section by $\sigma_{\chi\mathcal{N}}^{\text{SI}} = \mu_N^2 |c_+^M|^2 / \pi$, with reduced mass μ_N . Ideally, to go beyond this approximation a global correlated analysis of direct-detection experiments based on either Eq. (1) or Eq. (2) should be performed in order to determine limits on all parameters at once, which, however, would require the consideration of more than one target nucleus in the analysis.

Barring such a global analysis, one would need to consider slices through the BSM parameter space, e.g., in terms of scans over the Wilson coefficients as in Ref. [39]. Such slices through the parameter space could also be organized in a straightforward extension of present analyses by considering one nuclear response at a time (this is, setting all but one c to zero), for instance based on Eq. (2), with four c parameters [which map onto seven (four) Wilson coefficients for a Dirac (Majorana) WIMP]. This would allow one to set limits on different combinations of Wilson coefficients. In particular, due to the role of the two-body responses this kind of analysis would extend the sensitivity of direct-detection experiments to more new-physics couplings than the standard SI single-nucleon cross section studied so far. Depending on the sensitivity of the experiment to the \mathbf{q}^2 -dependence, the number of relevant structure factors may be reduced, and limits could also be obtained for combinations of the coefficients associated with responses with similar \mathbf{q}^2 -tail, e.g., \mathcal{F}_π and \mathcal{F}_π^θ . In that case the one-response-at-a-time analysis could also be

performed based on Eq. (1), which originally depends on eight nonindependent c coefficients.

In conclusion, we provide a parametrization of the WIMP-nucleus cross section for general SI scattering, which could be applied to generalize the extraction of limits from SI scattering beyond the standard $\sigma_{\chi\mathcal{N}}^{\text{SI}}$ cross section (corresponding to c_+^M), e.g., by similar exclusion plots for the additional coefficients in the minimal four-parameter extension in Eq. (2), or by more sophisticated scans through the BSM parameter space. For a xenon target, all necessary structure factors are provided in Secs. IV and V.

III. FORMALISM

We consider a WIMP χ scattering off a target nucleus \mathcal{N} with momenta assigned as

$$\mathcal{N}(p) + \chi(k) \rightarrow \mathcal{N}(p') + \chi(k'), \quad (3)$$

and momentum transfer

$$q = k' - k = p - p', \quad q^2 = t, \quad (4)$$

as well as

$$P = p + p', \quad K = k + k'. \quad (5)$$

The rate for the detection of a dark-matter particle χ scattering elastically off a nucleus with mass number A , differential in the three-momentum transfer \mathbf{q} , is then given by

$$\frac{dR}{d\mathbf{q}^2} = \frac{\rho M}{m_A m_\chi} \int_{v_{\min}}^{v_{\text{esc}}} d^3v |\mathbf{v}| f(|\mathbf{v}|) \frac{d\sigma_{\chi\mathcal{N}}}{d\mathbf{q}^2}, \quad (6)$$

where M denotes the (fiducial) mass of the experiment, m_A and m_χ the masses of target nucleus and WIMP, respectively, $\sigma_{\chi\mathcal{N}}$ the WIMP-nucleus cross section in the lab frame, $f(|\mathbf{v}|)$ the normalized velocity distribution of the WIMP, ρ the WIMP density, $v_{\text{esc}} = 544_{-46}^{+64}$ km s⁻¹ [41] the escape velocity of our galaxy, and

$$\begin{aligned} v_{\min}^2 &= -t \left[\frac{\sqrt{4m_A^2 - t} + \sqrt{4m_\chi^2 - t}}{\sqrt{4m_A^2 - t} \sqrt{4m_\chi^2 - t - t}} \right]^2 \\ &= \frac{\mathbf{q}^2}{4\mu_A^2} + \mathcal{O}(\mathbf{q}^4), \\ \mu_A &= \frac{m_A m_\chi}{m_A + m_\chi}, \end{aligned} \quad (7)$$

with $t = -\mathbf{q}^2$ up to relativistic corrections. The value for the local WIMP density canonically used in the interpretation of direct-detection experiments is $\rho = 0.3$ GeV/cm³,

although halo-independent methods have been developed that allow one to eliminate the astrophysical uncertainties in the comparison of different experiments, see, e.g., Refs. [42,43]. Alternatively, the detection rate Eq. (6) is often formulated differential in the recoil energy

$$E_r = \frac{\mathbf{q}^2}{2m_A}. \quad (8)$$

The WIMP-nucleus cross section itself combines physics from particle, hadronic, and nuclear scales. To separate the nuclear contributions, $\sigma_{\chi N}$ can be expressed in terms of structure factors [22]

$$\frac{d\sigma_{\chi N}}{d\mathbf{q}^2} = \frac{8G_F^2}{v^2(2J+1)} [S_S(\mathbf{q}^2) + S_A(\mathbf{q}^2)], \quad (9)$$

where J refers to the spin of the target nucleus, G_F denotes the Fermi constant, and S_S and S_A are the structure factors for SI and SD scattering, respectively. These structure factors are normalized according to

$$\begin{aligned} S_S(0) &= \frac{2J+1}{4\pi} |c_0 A + c_1(Z-N)|^2, \\ S_A(0) &= \frac{(2J+1)(J+1)}{4\pi J} \\ &\quad \times |(a_0 + a_1)\langle \mathbf{S}_p \rangle + (a_0 - a_1)\langle \mathbf{S}_n \rangle|^2, \end{aligned} \quad (10)$$

with proton and neutron numbers Z and N ($A = Z + N$) and proton/neutron spin expectation values $\langle \mathbf{S}_{p/n} \rangle$. The constants c_i , a_i contain the information about particle and hadronic physics, a relation to be made more precise below. Assuming $c_1 = 0$, the cross section for SI scattering is often represented in the standard form [44]

$$\frac{d\sigma_{\chi N}^{\text{SI}}}{d\mathbf{q}^2} = \frac{\sigma_{\chi N}^{\text{SI}}}{4v^2\mu_N^2} \mathcal{F}_{\text{SI}}^2(\mathbf{q}^2), \quad \mu_N = \frac{m_N m_\chi}{m_N + m_\chi}, \quad (11)$$

with nucleon mass m_N and single-nucleon cross section $\sigma_{\chi N}^{\text{SI}}$. The nuclear-physics quantity $\mathcal{F}_{\text{SI}}(\mathbf{q}^2)$ is the only remnant of the structure factor, and is frequently approximated by [45]

$$\begin{aligned} \mathcal{F}_{\text{SI}}^{\text{Helm}}(\mathbf{q}^2) &= A \frac{3j_1(|\mathbf{q}|r_n)}{|\mathbf{q}|r_n} e^{-\frac{1}{2}\mathbf{q}^2 s^2}, \\ r_n^2 &= c^2 + \frac{7}{3}\pi^2 a^2 - 5s^2, \\ s &= 1 \text{ fm}, \\ c &= (1.23A^{1/3} - 0.60) \text{ fm}, \\ a &= 0.52 \text{ fm}, \end{aligned} \quad (12)$$

whose square is known as Helm form factor.

In the following, we revisit this formalism starting from an effective Lagrangian for the interaction of the WIMP with Standard-Model fields presented in Sec. III A. In Secs. III B and III C we discuss the relevant nucleon couplings and finally in Sec. III D we derive a generalized decomposition for SI scattering that includes two-body currents and the nuclear Φ'' response.

A. Lagrangian and Wilson coefficients

We consider the following dimension-6 and -7 effective Lagrangian for the interaction of a spin-1/2 WIMP with quark and gluon fields

$$\begin{aligned} \mathcal{L}_\chi &= \mathcal{L}_\chi^{(6)} + \mathcal{L}_\chi^{(7)}, \\ \mathcal{L}_\chi^{(6)} &= \frac{1}{\Lambda^2} \sum_q [C_q^{VV} \bar{\chi} \gamma^\mu \chi \bar{q} \gamma_\mu q + C_q^{AA} \bar{\chi} \gamma^\mu \gamma_5 \chi \bar{q} \gamma_\mu \gamma_5 q], \\ \mathcal{L}_\chi^{(7)} &= \frac{1}{\Lambda^3} \sum_q C_q^{SS} \bar{\chi} \chi m_q \bar{q} q + \frac{1}{\Lambda^3} C_g^{S} \bar{\chi} \chi \alpha_s G_{\mu\nu}^a G_{\mu\nu}^a \\ &= \frac{1}{\Lambda^3} \sum_q \left(C_q^{SS} + \frac{8\pi}{9} C_g^{S} \right) \bar{\chi} \chi m_q \bar{q} q \\ &\quad - \frac{8\pi}{9} \frac{1}{\Lambda^3} C_g^{S} \bar{\chi} \chi \theta_\mu^\mu, \end{aligned} \quad (13)$$

where χ is assumed to be a Standard-Model singlet, the quark masses m_q have been included to make the scalar operator renormalization-group invariant, and the Wilson coefficients C_i parametrize the BSM physics associated with the scale Λ . The effective Lagrangian is defined at the hadronic scale, with the quark sum extending over $q = u, d, s$, after the heavy quarks have been integrated out and their effect has been absorbed into a redefinition of the gluon coefficient C_g^S , see Eq. (16). In the second formulation of the dimension-7 Lagrangian the gluon term has been replaced in favor of the trace of the QCD energy-momentum tensor θ_μ^μ . Equation (13) includes the leading operators relevant for coherent WIMP-nucleus scattering, vector and scalar channels, but also retains the axial-vector operator to facilitate the comparison to the SD case. The WIMP could either be a Dirac or Majorana particle, with $C_q^{VV} = 0$ in the latter case. At dimension 8, there are spin-2 operators that can become relevant for the SI scattering of heavy WIMPs [46], but their inclusion will be left for future work. Similarly, the operator basis changes for different quantum numbers of the WIMP [46,47].

Throughout this work we follow the chiral counting formulated in Refs. [35,37] to organize the calculation. In particular, this implies that momentum corrections to the one-body matrix elements occurring in Eq. (13) enter at the same order as the leading two-body contributions, at third order in ChEFT [37]. The nucleon matrix elements of the operators listed in Eq. (13) involve a combination of Wilson coefficients and nucleon couplings. In the next sections, we

spell out these combinations, closely following the notation introduced in Ref. [37].

B. Scalar couplings

For the scalar channel in Eq. (13) we need the following coupling to the nucleon ($N = n$ or p):

$$f_N(t) = \frac{m_N}{\Lambda^3} \left(\sum_{q=u,d,s} C_q^{SS} f_q^N(t) - 12\pi f_Q^N(t) C_g^{S} \right), \quad (14)$$

where the nucleon scalar form factors are defined as

$$m_N f_q^N(t) = \langle N(p') | m_q \bar{q} q | N(p) \rangle. \quad (15)$$

The form factors for the heavy quarks $f_Q^N(t)$ appear together with the modified gluon Wilson coefficient

$$C_g^{S} = C_g^S - \frac{1}{12\pi} \sum_{Q=c,b,t} C_Q^{SS} \quad (16)$$

after integrating out their effect by means of the trace anomaly of the energy-momentum tensor $\theta_{\mu\nu}$ [48], which also produces

$$f_Q^N(t) = \frac{2}{27} \left(\frac{\theta_0^N(t)}{m_N} - \sum_{q=u,d,s} f_q^N(t) \right),$$

$$\theta_0^N(t) = \langle N(p') | \theta_\mu^\mu | N(p) \rangle. \quad (17)$$

It should be noted that this procedure is accurate at $\mathcal{O}(\alpha_s)$, which may not be sufficient for the c quark, see Refs. [46,49,50] for a study of higher orders in α_s .

We begin with the discussion of Eq. (14) at vanishing momentum transfer, in which case the form factors simply reduce to the scalar couplings of the nucleon. Based on $SU(2)$ chiral perturbation theory (ChPT), it can be shown that the couplings to u and d quarks only depend on the value of the pion-nucleon σ -term $\sigma_{\pi N}$, while isospin-breaking corrections are fully determined by the same low-energy constant that governs the strong contribution to the proton-neutron mass difference [51]. Combining dispersive techniques [52] with precision data for the pion-nucleon scattering lengths extracted from pionic atoms [53,54] leads to the phenomenological values [55] for the light-quark couplings quoted in the first line of Table I.

TABLE I. Scalar u and d couplings of the nucleon, in units of 10^{-3} .

f_u^p	f_u^n	f_d^p	f_d^n	References
20.8(1.5)	18.9(1.4)	41.1(2.8)	45.1(2.7)	[55]
13.9(1.8)	11.6(1.7)	25.3(3.7)	30.2(3.8)	[56]

TABLE II. Scalar s coupling of the nucleon, in units of 10^{-3} .

f_s^N	113(60)	34(7)	44(9)	37(13)	43(11)
References	[56]	[57]	[58]	[59]	[61]

More recently, lattice calculations at physical quark masses have produced significantly lower values for $\sigma_{\pi N}$ [56–59], which translates to the 3σ tension in the scalar couplings shown in Table I. This tension between phenomenology and lattice [60] currently constitutes the largest uncertainty in the u and d couplings.

In contrast to the u and d quarks, a determination of the scalar coupling to the s quark from phenomenology requires the use of $SU(3)$ relations, whose convergence properties make reliable uncertainty estimates difficult. For this reason, in Table II we only quote the values obtained by recent lattice calculations, together with the average from Ref. [61] of previous lattice results. In particular, we assume isospin symmetry $f_q^p = f_q^n$ for $q = s, c, b, t$. Finally, Ref. [58] also provides a value for the c coupling, $f_c^N = 0.085(22)$, to be compared with $f_Q^N = 0.068(1)$ as extracted from the same reference based on Eq. (17) [with $\theta_0^N(0) = m_N$]. Within uncertainties, the direct determination from lattice QCD thus agrees with the result extracted by means of the trace anomaly at $\mathcal{O}(\alpha_s)$.

Next, we turn to the finite-momentum-transfer corrections to $f_N(0) \equiv f_N$.¹ To the order we are working in ChEFT, it is generally sufficient to keep the radius corrections, i.e., the first order in the expansion around $t = 0$. However, the strong $\pi\pi$ rescattering in the isospin-0 $\pi\pi$ S -wave makes the leading-loop ChPT prediction for the slope of the scalar form factor of the nucleon at $t = 0$ [62],

$$\dot{\sigma}|_{\text{ChPT}} = \frac{5g_A^2 M_\pi}{256\pi F_\pi^2} = 0.17 \text{ GeV}^{-1}, \quad (18)$$

underestimate the true result by nearly a factor of 2 [$g_A = 1.2723(23)$ and $F_\pi = 92.2(2)$ MeV are taken from Ref. [63]]. For this reason, we make use of the updated dispersive analysis from Refs. [64,65] and use

$$\dot{\sigma} = 0.27(1) \text{ GeV}^{-1}. \quad (19)$$

Retaining the leading isospin-breaking effect, this correction amounts to the replacement

$$f_u^N(t) \rightarrow f_u^N + \frac{1-\xi}{2m_N} \dot{\sigma} t, \quad \xi = \frac{m_d - m_u}{m_d + m_u} = 0.37(3),$$

$$f_d^N(t) \rightarrow f_d^N + \frac{1+\xi}{2m_N} \dot{\sigma} t, \quad (20)$$

where we have used $m_u/m_d = 0.46(3)$ [66].

¹Here and below, couplings without argument are understood to be evaluated at $t = 0$.

In analogy to Eq. (18), there is a parameter-free prediction from leading-loop $SU(3)$ ChPT for the slope of the strangeness radius [35]

$$\begin{aligned} \dot{\sigma}_s|_{\text{ChPT}} &= \frac{5g_A^2}{256\pi F_\pi^2} \left(M_K^2 - \frac{1}{2} M_\pi^2 \right) \frac{1}{3} \left\{ \frac{4}{3M_\eta} \left(\frac{1-4\alpha}{\sqrt{3}} \right)^2 \right. \\ &\quad \left. + \frac{1}{M_K} \left[3(1-2\alpha)^2 + \left(\frac{1+2\alpha}{\sqrt{3}} \right)^2 \right] \right\} \\ &= 0.24 \text{ GeV}^{-1}, \end{aligned} \quad (21)$$

where $\alpha = F/(D+F)$ parametrizes the leading $SU(3)$ couplings. Numerically, we use $F/D = 0.57$ as extracted from semileptonic hyperon decays [67,68], which together with the $SU(2)$ constraint $D+F = g_A$ implies

$$D = 0.81, \quad F = 0.46, \quad \alpha = 0.36. \quad (22)$$

However, such $SU(3)$ leading-loop low-energy theorems are known to be sensitive to higher-order corrections [69,70]. Therefore, we also considered the coupled-channel dispersive analysis [64], which in principle provides not only a prediction for $\dot{\sigma}$ but also for $\dot{\sigma}_s$. Unfortunately, convergence of the dispersive integrals is much slower for the slope of the strangeness form factor, although the resulting values are not too far from the chiral prediction. All in all, the spread observed in both methods would be covered by a range

$$\dot{\sigma}_s = 0.3(2) \text{ GeV}^{-1}, \quad (23)$$

leading to

$$f_s^N(t) \rightarrow f_s^N + \frac{\dot{\sigma}_s}{m_N} t. \quad (24)$$

In view of the substantial uncertainties already encountered in the strangeness form factor, we do not make an attempt to quantify radius corrections for the heavy quarks. The leading chiral result, however, can be reconstructed by means of Eq. (17) and

$$\theta_0^N(t) = m_N - \frac{13g_A^2 M_\pi}{128\pi F_\pi^2} t + \mathcal{O}(t^2). \quad (25)$$

Taking everything together, we arrive at the following decomposition of the combination of Wilson coefficients and nucleon form factors relevant for the scalar channel

$$\begin{aligned} f_N(t) &= f_N + t\dot{f}_N + \mathcal{O}(t^2), \\ f_N &= \frac{m_N}{\Lambda^3} \left(\sum_{q=u,d,s} C_q^{SS} f_q^N - 12\pi f_Q^N C_g^{S'} \right), \\ \dot{f}_N &= \frac{1}{\Lambda^3} \left(C_u^{SS} \frac{1-\xi}{2} \dot{\sigma} + C_d^{SS} \frac{1+\xi}{2} \dot{\sigma} + C_s^{SS} \dot{\sigma}_s \right). \end{aligned} \quad (26)$$

For the scalar two-body matrix element we also need the couplings to the pion

$$\begin{aligned} f_\pi &= \frac{M_\pi}{\Lambda^3} \sum_{q=u,d} \left(C_q^{SS} + \frac{8\pi}{9} C_g^{S'} \right) f_q^\pi, \\ f_\pi^\theta &= -\frac{M_\pi}{\Lambda^3} \frac{8\pi}{9} C_g^{S'}, \end{aligned} \quad (27)$$

with

$$\begin{aligned} f_u^\pi &= \frac{m_u}{m_u + m_d} = \frac{1}{2} (1 - \xi) = 0.32(2), \\ f_d^\pi &= \frac{m_d}{m_u + m_d} = \frac{1}{2} (1 + \xi) = 0.68(2). \end{aligned} \quad (28)$$

In Eq. (27) we introduced a factor M_π in analogy to the scalar coupling to the nucleon, Eq. (14). The necessity of defining two pion couplings, f_π and f_π^θ in Eq. (27), traces back to the fact that the couplings of the scalar current $m_q \bar{q}q$ and the trace anomaly of the energy-momentum tensor θ_μ^μ to the pion differ qualitatively: while the former is constant up to higher-order corrections, the latter becomes momentum dependent and therefore produces a different nuclear structure factor.

C. Vector and axial-vector couplings

In the vector channel there are two sets of couplings to the nucleon

$$f_i^{V,N}(t) = \frac{1}{\Lambda^2} \sum_{q=u,d,s} C_q^{VV} F_i^{q,N}(t), \quad (29)$$

with $i = 1, 2$ related to the Dirac and Pauli terms, respectively, in the decomposition of the nucleon form factors of the electromagnetic current. A decomposition analogous to Eq. (26) is given by

$$\begin{aligned} f_1^{V,N}(t) &= f_1^{V,N} + t\dot{f}_1^{V,N} + \mathcal{O}(t^2), \\ f_2^{V,N}(t) &= f_2^{V,N} + \mathcal{O}(t). \end{aligned} \quad (30)$$

Since the matrix element of the Pauli form factor vanishes at zero momentum transfer, the leading term in $f_2^{V,N}(t)$ is sufficient. Assuming isospin symmetry (for corrections see Ref. [71]), these couplings expressed in terms of nucleon radii and anomalous magnetic moments become [37]

TABLE III. Nucleon radii and anomalous magnetic moments. The values of κ_p , κ_n , and $\langle r_E^2 \rangle^n$ are taken from Ref. [63], $\langle r_E^2 \rangle^p$ from Ref. [72], and κ_N^s as well as $\langle r_{E,s}^2 \rangle^N$ from a global analysis of parity-violating asymmetry data [73]. Note that the latter two are strongly correlated, with a correlation coefficient 0.87.

κ_p	κ_n	κ_N^s
1.792847356(23)	-1.91304272(45)	-0.26(26)
$\langle r_E^2 \rangle^p$	$\langle r_E^2 \rangle^n$	$\langle r_{E,s}^2 \rangle^N$
0.7071(7) fm ²	-0.1161(22) fm ²	-0.06(4) fm ²

$$\begin{aligned}
 f_1^{V,p} &= \frac{1}{\Lambda^2} (2C_u^{VV} + C_d^{VV}), \\
 f_2^{V,p} &= \frac{1}{\Lambda^2} [(2C_u^{VV} + C_d^{VV})\kappa_p + (C_u^{VV} + 2C_d^{VV})\kappa_n \\
 &\quad + (C_u^{VV} + C_d^{VV} + C_s^{VV})\kappa_N^s], \\
 \dot{f}_1^{V,p} &= \frac{1}{\Lambda^2} \left[(2C_u^{VV} + C_d^{VV}) \left(\frac{\langle r_E^2 \rangle^p}{6} - \frac{\kappa_p}{4m_p^2} \right) \right. \\
 &\quad + (C_u^{VV} + 2C_d^{VV}) \left(\frac{\langle r_E^2 \rangle^n}{6} - \frac{\kappa_n}{4m_n^2} \right) \\
 &\quad \left. + (C_u^{VV} + C_d^{VV} + C_s^{VV}) \left(\frac{\langle r_{E,s}^2 \rangle^N}{6} - \frac{\kappa_N^s}{4m_N^2} \right) \right], \quad (31)
 \end{aligned}$$

and $u \leftrightarrow d$ for the neutron couplings. Numerical values for the nucleon radii and anomalous magnetic moments are collected in Table III.

For completeness, we also quote the analogous decomposition for the axial-vector channel appearing in Eq. (13). In this case, one needs the combinations $g_A^N(t)$ and $g_P^N(t)$ with

$$\begin{aligned}
 g_A^N(t) &= g_A^N + t\dot{g}_A^N + \mathcal{O}(t^2), \\
 g_A^N &= \frac{1}{\Lambda^2} \left[\pm \frac{g_A}{2} (C_u^{AA} - C_d^{AA}) \right. \\
 &\quad + \frac{3F-D}{6} (C_u^{AA} + C_d^{AA} - 2C_s^{AA}) \\
 &\quad \left. + \frac{\Delta\Sigma^N}{3} (C_u^{AA} + C_d^{AA} + C_s^{AA}) \right], \\
 \dot{g}_A^N &= \pm \frac{g_A}{\Lambda^2} (C_u^{AA} - C_d^{AA}) \frac{1}{M_A^2}, \\
 g_P^N(t) &= -\frac{4m_N^2}{\Lambda^2} \left[\pm \frac{g_A}{2} (C_u^{AA} - C_d^{AA}) \frac{1}{t - M_\pi^2} \right. \\
 &\quad \left. + \frac{3F-D}{6} (C_u^{AA} + C_d^{AA} - 2C_s^{AA}) \frac{1}{t - M_\eta^2} \right], \quad (32)
 \end{aligned}$$

where the upper/lower sign refers to proton/neutron and the small η contribution of the last line above is generally neglected in SD analyses. These relations involve the nucleon spin matrix elements $\Delta q^N = \langle N | \bar{q} \gamma_\mu \gamma_5 q | N \rangle / \langle N | \gamma_\mu \gamma_5 | N \rangle$,

for which we have assumed isospin symmetry and already used the combinations

$$\begin{aligned}
 g_A &= \Delta u^p - \Delta d^p = \Delta d^n - \Delta u^n, \\
 3F - D &= \Delta u^N + \Delta d^N - 2\Delta s^N, \\
 \Delta\Sigma^N &= \Delta u^N + \Delta d^N + \Delta s^N. \quad (33)
 \end{aligned}$$

Due to the axial anomaly, the singlet combination $\Delta\Sigma^N$ cannot be analyzed in $SU(3)$ ChPT, as effects related to the η' will play a role. However, it can be extracted from the spin structure function of the nucleon, which, at $Q^2 = 5$ GeV² and to order $\mathcal{O}(\alpha_s^2)$, produces $\Delta\Sigma^N = 0.330(39)$ [74]. Further, the dominant radius correction occurring in the isovector contribution in Eq. (32) has been included by a dipole ansatz with mass parameter M_A around 1 GeV [75,76], while the pseudoscalar poles in $g_P^N(t)$ prevent a Taylor expansion in t .

D. Structure factors

For the definition of the nuclear structure factors we first consider the matching of the one-body operators obtained in ChEFT above onto the NREFT basis of Refs. [26,28]. This produces the matrix elements

$$\begin{aligned}
 \mathcal{M}_{1,\text{NR}}^{SS} &= \mathcal{O}_1 f_N(t), \\
 \mathcal{M}_{1,\text{NR}}^{VV} &= \mathcal{O}_1 \left(f_1^{V,N}(t) + \frac{t}{4m_N^2} f_2^{V,N}(t) \right) \\
 &\quad + \frac{1}{m_N} \mathcal{O}_3 f_2^{V,N}(t), \\
 \mathcal{M}_{1,\text{NR}}^{AA} &= -4\mathcal{O}_4 g_A^N(t) + \frac{1}{m_N^2} \mathcal{O}_6 g_P^N(t), \quad (34)
 \end{aligned}$$

where we have dropped the nucleon and WIMP spinors.² The NREFT operators \mathcal{O}_i are defined by

$$\begin{aligned}
 \mathcal{O}_1 &= 1, \\
 \mathcal{O}_3 &= i\mathbf{S}_N \cdot (\mathbf{q} \times \mathbf{v}^\perp), \\
 \mathcal{O}_4 &= \mathbf{S}_\chi \cdot \mathbf{S}_N, \\
 \mathcal{O}_6 &= \mathbf{S}_\chi \cdot \mathbf{q} \mathbf{S}_N \cdot \mathbf{q}, \quad (35)
 \end{aligned}$$

with spins $\mathbf{S} = \boldsymbol{\sigma}/2$ and velocity

$$\mathbf{v}^\perp = \frac{\mathbf{K}}{2m_\chi} - \frac{\mathbf{P}}{2m_N}. \quad (36)$$

²For details see Ref. [37]. This matching is performed at tree level and hence does not include effects from operator evolution, which could be generated when running the ChEFT operators down to nuclear scales.

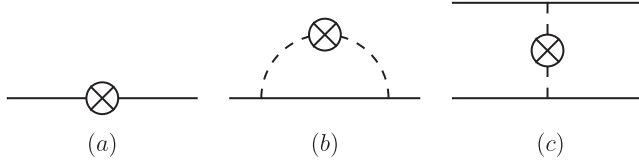


FIG. 2. Diagrams for WIMP-nucleon interactions in ChEFT. Solid (dashed) lines denote nucleons (pions) and crosses the coupling to the WIMP current. Diagram (a) represents a leading one-body term, (b) a radius correction, and (c) a two-body current.

The combination of the different operators in Eq. (34) demonstrates how QCD constraints impose relations between the NREFT operators: for the axial-vector channel it is a fixed combination of \mathcal{O}_4 and \mathcal{O}_6 that contributes, while the same coefficient $f_2^{V,N}(t)$ that multiplies \mathcal{O}_3 also appears as a momentum-dependent correction to \mathcal{O}_1 .

In Eq. (34) we only retained those channels that generate coherent or quasicohherent nuclear responses, compared to the full list studied in Ref. [37]. These coherent and quasicohherent responses are denoted as M and Φ'' in Refs. [26,28], and are only a subset of the six different nuclear responses generated by the NREFT operators, which also include the Σ' , Σ'' , Δ , and $\tilde{\Phi}'$ responses. For example, M governs standard SI scattering, and it is a combination of Σ' and Σ'' that enters in SD scattering.

Beyond the single-nucleon sector, NREFT operators that involve \mathbf{v}^\perp can be decomposed into two parts [26,28]. First, there are terms proportional to the relative WIMP velocity with respect to the center of mass of the nucleus

$$\mathbf{v}_T^\perp = \frac{\mathbf{K}}{2m_\chi} - \frac{1}{A} \sum_{i=1}^A \frac{\mathbf{P}_i}{2m_N}, \quad (37)$$

where $\mathbf{P}_i = \mathbf{p}_i + \mathbf{p}'_i$ is the sum of the initial and final nucleon momenta. These terms are effectively suppressed by the WIMP velocity with respect to the target $|\mathbf{v}_T^\perp| \approx 10^{-3}$ and will thus be neglected in the following. Second, \mathbf{v}^\perp also produces contributions involving the velocity operator of the nucleon, which are part of the Δ , $\tilde{\Phi}'$, and Φ'' responses and come with a milder suppression factor $|\mathbf{q}|/m_N$. This is the case for the \mathcal{O}_3 contribution kept in Eq. (34), which generates a Φ'' response. In the end, for coherent SI scattering only scalar and vector interactions remain, and the fact that the Φ'' response is due only to the vector operator could serve as a tool to discriminate between these two channels.

Apart from the one-body operators and the momentum corrections as summarized in Secs. III B and III C, there are two-body currents at the same order in ChEFT, see Fig. 2. The corresponding NR amplitudes take the form

$$\begin{aligned} \mathcal{M}_{2,\text{NR}}^{SS} &= - \left(\frac{g_A}{2F_\pi} \right)^2 f_\pi M_\pi \frac{\boldsymbol{\tau}_1 \cdot \boldsymbol{\tau}_2 \boldsymbol{\sigma}_1 \cdot \mathbf{q}_1 \boldsymbol{\sigma}_2 \cdot \mathbf{q}_2}{(\mathbf{q}_1^2 + M_\pi^2)(\mathbf{q}_2^2 + M_\pi^2)}, \\ \mathcal{M}_{2,\text{NR}}^\theta &= \frac{4M_\pi^2 - 2\mathbf{q}_1 \cdot \mathbf{q}_2}{M_\pi^2} \frac{f_\pi^\theta}{f_\pi} \mathcal{M}_{2,\text{NR}}^{SS}, \end{aligned} \quad (38)$$

where f_π and f_π^θ are defined in Eq. (27), $\boldsymbol{\sigma}_i$ and $\boldsymbol{\tau}_i$ denote the spin and isospin Pauli matrices of nucleon i , respectively, and $\mathbf{q}_i = \mathbf{p}'_i - \mathbf{p}_i$. Diagrammatically, these amplitudes represent the coupling of the WIMP to the pion in flight via a scalar current and by means of the QCD trace anomaly θ_μ^μ . The other two-body currents identified in Ref. [37] in general involve isospin operators $[\boldsymbol{\tau}_1 \times \boldsymbol{\tau}_2]^3$ as well as spin structures that, after summing over spins, make the diagrams vanish. The only remaining contribution is the exchange diagram from the axial-vector–vector channel, whose isospin structure becomes $\boldsymbol{\tau}_1^3 - \boldsymbol{\tau}_2^3$, only allowing for an isovector coherent enhancement suppressed by $(N - Z)/A$ with respect to the scalar two-body current. In addition, this two-body current is linear in \mathbf{S}_χ and does not interfere with \mathcal{O}_1 [26]. Other contributions such as the vector-vector two-body current also show isovector coherent enhancement only, and are further suppressed in the ChEFT expansion [37]. For these reasons, we restrict our analysis to the contributions given by Eq. (38). It is the presence of the $\mathbf{q}_1 \cdot \mathbf{q}_2$ term in the relation between quark-mass and trace-anomaly couplings that necessitates the definition of two structure factors: for a constant term, the θ_μ^μ contribution could be absorbed into a redefinition of f_π , similarly to f_N in the case of the nucleon coupling [see Eqs. (14) and (17)].

In this context, several comments on the role of two-body operators are in order. First, the hierarchy of diagrams shown in Fig. 2 assumes the ChEFT counting originally proposed by Weinberg [77,78]. In this counting, the coupling of the scalar current to $(N^\dagger N)^2$ contact operators is suppressed by two orders in the chiral expansion. Due to the limitations of Weinberg counting, this suppression might be less pronounced in practice, as indicated, e.g., by Kaplan-Savage-Wise (KSW) counting [79,80] or by general arguments related to the short-range behavior of nucleon-nucleon wave functions [81]. The role of such contact operators at heavy pion masses has been studied in Ref. [82] using lattice QCD, and calculations at or close to the physical pion mass would allow for a check of the ChEFT counting employed here.

Second, while diagram (a) corresponds directly to an NREFT operator from Refs. [26,28], the mapping of diagrams (b) and (c) would proceed in an indirect way. The radius corrections (b) are represented by \mathbf{q} -dependent prefactors of the \mathcal{O}_i , see Eq. (34). The two-body contributions (c) could be modeled as effective one-body operators, if summed over the second nucleon with respect to a given reference state, symbolically written as $\langle N^\dagger N \rangle N^\dagger N$, so that the effective one-body operator would

become density and state dependent. Such a normal-ordering approximation with respect to a Fermi gas was used in the context of SD scattering [36,38]. However, in this work we perform a full calculation in harmonic-oscillator basis states, see Sec. V. It is the explicit calculation of all diagrams (a)–(c) within ChEFT, instead of a parametrization in terms of effective one-body operators, which allows one to relate the coefficients of the nuclear structure factors to nucleon form factors and new-physics parameters.

For the construction of suitable nuclear structure factors for generalized SI scattering, we first turn to the SD case. Here the result in Eq. (32) shows that once the η contribution to $g_p^N(t)$ is neglected, only two independent combinations of Wilson coefficients remain, which can be conveniently identified with the coefficients introduced in Eq. (10):

$$\begin{aligned} a_0 &= \frac{\zeta}{2\sqrt{2}G_F\Lambda^2} \\ &\quad \times [(C_u^{AA} + C_d^{AA})(\Delta u^N + \Delta d^N) + 2C_s^{AA}\Delta s^N] \\ &= \frac{\zeta}{6\sqrt{2}G_F\Lambda^2} [(3F - D)(C_u^{AA} + C_d^{AA} - 2C_s^{AA}) \\ &\quad + 2\Delta\Sigma(C_u^{AA} + C_d^{AA} + C_s^{AA})], \\ a_1 &= \frac{\zeta}{2\sqrt{2}G_F\Lambda^2} (C_u^{AA} - C_d^{AA})(\Delta u^p - \Delta d^p) \\ &= \frac{\zeta g_A}{2\sqrt{2}G_F\Lambda^2} (C_u^{AA} - C_d^{AA}), \end{aligned} \quad (39)$$

where $\zeta = 1(2)$ for a Dirac (Majorana) spin-1/2 WIMP. The structure factor can therefore be decomposed as

$$S_A(\mathbf{q}^2) = a_0^2 S_{00}(\mathbf{q}^2) + a_0 a_1 S_{01}(\mathbf{q}^2) + a_1^2 S_{11}(\mathbf{q}^2), \quad (40)$$

or, in terms of so-called proton-only and neutron-only structure factors,

$$\begin{aligned} S_A^p(\mathbf{q}^2) &= S_{00}(\mathbf{q}^2) + S_{01}(\mathbf{q}^2) + S_{11}(\mathbf{q}^2), \\ S_A^n(\mathbf{q}^2) &= S_{00}(\mathbf{q}^2) - S_{01}(\mathbf{q}^2) + S_{11}(\mathbf{q}^2). \end{aligned} \quad (41)$$

Since both the momentum corrections in Eq. (32) and the leading two-body currents [38] also depend on a_0 and a_1 only, this implies that the definition of the structure factors Eq. (40) remains applicable even once such corrections are included. In fact, in a normal-ordering approximation the effect from two-body currents amounts to a shift $a_1 \rightarrow a_1(1 + \Delta a_1)$, with Δa_1 predicted from ChEFT. The connection between experimental limits for the direct-detection rate and the Wilson coefficients therefore still proceeds by means of Eq. (39).

Our aim is to find a similar decomposition for SI scattering. More precisely, we wish to formulate a set of structure factors that captures the leading corrections,

taking into account both the ChEFT expansion and coherence effects in the nucleus, in particular including both one- and two-body operators.

As a first step towards the construction of generalized SI structure factors, we again identify the couplings at vanishing momentum transfer. In this limit we obtain

$$\begin{aligned} c_0 &= \frac{\zeta}{4\sqrt{2}G_F} (f_p + f_n + f_1^{V,p} + f_1^{V,n}), \\ c_1 &= \frac{\zeta}{4\sqrt{2}G_F} (f_p - f_n + f_1^{V,p} - f_1^{V,n}). \end{aligned} \quad (42)$$

Indeed, for $f_p = f_n = f_N$, $f_1^{V,p} = f_1^{V,n} = f_1^{V,N}$ the single-nucleon cross section at threshold becomes

$$\sigma_{\chi N}^{\text{SI}} = \frac{\zeta^2 \mu_N^2}{\pi} |f_N + f_1^{V,N}|^2, \quad (43)$$

leading to the simplification anticipated in Eq. (11). Limits for $\sigma_{\chi N}^{\text{SI}}$ should therefore be interpreted as limits on the combination of Wilson coefficients given by $f_N + f_1^{V,N}$, under the assumption that proton and neutron couplings are identical.

Based on the previous discussion we propose the following decomposition for the WIMP-nucleus differential cross section:

$$\begin{aligned} \frac{d\sigma_{\chi N}^{\text{SI}}}{d\mathbf{q}^2} &= \frac{\zeta^2}{4\pi\mathbf{v}^2} \left[f_+^M(\mathbf{q}^2) \mathcal{F}_+^M(\mathbf{q}^2) + f_-^M(\mathbf{q}^2) \mathcal{F}_-^M(\mathbf{q}^2) \right. \\ &\quad + \frac{\mathbf{q}^2}{2m_N^2} [f_+^{\Phi''} \mathcal{F}_+^{\Phi''}(\mathbf{q}^2) + f_-^{\Phi''} \mathcal{F}_-^{\Phi''}(\mathbf{q}^2)] \\ &\quad \left. + f_\pi \mathcal{F}_\pi(\mathbf{q}^2) + f_\pi^\theta \mathcal{F}_\pi^\theta(\mathbf{q}^2) \right]^2, \end{aligned} \quad (44)$$

where

$$\begin{aligned} f_\pm^M(\mathbf{q}^2) &= \frac{1}{2} \left[f_p \pm f_n - \mathbf{q}^2 (\dot{f}_p \pm \dot{f}_n) \right. \\ &\quad + f_1^{V,p} \pm f_1^{V,n} - \mathbf{q}^2 (\dot{f}_1^{V,p} \pm \dot{f}_1^{V,n}) \\ &\quad \left. - \frac{\mathbf{q}^2}{4m_N^2} (f_2^{V,p} \pm f_2^{V,n}) \right], \\ f_\pm^{\Phi''} &= \frac{1}{2} (f_2^{V,p} \pm f_2^{V,n}). \end{aligned} \quad (45)$$

The nuclear M responses in Eq. (44) are normalized to

$$\mathcal{F}_+^M(0) = A, \quad \mathcal{F}_-^M(0) = Z - N, \quad (46)$$

so that $\mathcal{F}_+^M(\mathbf{q}^2)$ coincides with the standard SI response $\mathcal{F}_{\text{SI}}^M(\mathbf{q}^2)$ in Eq. (11), and at vanishing momentum transfer is given by the combination of couplings that determines the single-nucleon cross section, see Eq. (43). In addition, $\mathcal{F}_-^M(\mathbf{q}^2)$ provides the corresponding isovector piece,

$\mathcal{F}_{\pm}^{\Phi''}(\mathbf{q}^2)$ is generated by the \mathcal{O}_3 operator in the vector channel, and $\mathcal{F}_{\pi}(\mathbf{q}^2)$ and $\mathcal{F}_{\pi}^{\theta}(\mathbf{q}^2)$ represent the two-body-current contributions. It is this decomposition in Eq. (44) that underlies the analysis strategy discussed in Sec. II. The nuclear response functions $\mathcal{F}_{\pm}^M(\mathbf{q}^2)$, $\mathcal{F}_{\pm}^{\Phi''}(\mathbf{q}^2)$, $\mathcal{F}_{\pi}(\mathbf{q}^2)$, and $\mathcal{F}_{\pi}^{\theta}(\mathbf{q}^2)$ are the subject of Secs. IV and V, where simple parametrizations are provided.

In Eq. (44) we used the interference pattern for the one-body pieces found in Refs. [26,28] for $L = 0$ multipoles, and extended it to include the two-body part. We assume this additional interference because the two-body terms come from a scalar operator with the same symmetry properties under parity and time reversal as \mathcal{O}_1 and \mathcal{O}_3 , and because these terms are independent of the WIMP spin \mathbf{S}_{χ} (interference terms vanish if they are linear in \mathbf{S}_{χ} [26]). Therefore, Eq. (44) neglects higher multipoles $L = 2$. These are only nonvanishing for ^{131}Xe (with a $J = 3/2$ ground state), but even in this case they are very small and not coherent, as shown in Ref. [40]. An expression similar to Eq. (44), only replacing the nuclear response functions \mathcal{F}_{\pm} , \mathcal{F}_{π} , $\mathcal{F}_{\pi}^{\theta}$ associated with $L = 0$ multipoles by the corresponding nuclear responses $\tilde{\mathcal{F}}_{\pm}$, $\tilde{\mathcal{F}}_{\pi}$, $\tilde{\mathcal{F}}_{\pi}^{\theta}$ for $L = 2$ can be added to the differential WIMP-nucleus cross section above.

In order to justify Eq. (44) we can consider the more general differential cross section which accommodates the contributions from all the NREFT operators that give rise to coherent or quasicohherent nuclear responses. This involves the additional operators

$$\mathcal{O}_5 = i\mathbf{S}_{\chi} \cdot (\mathbf{q} \times \mathbf{v}^{\perp}), \quad \mathcal{O}_8 = \mathbf{S}_{\chi} \cdot \mathbf{v}^{\perp}, \quad \mathcal{O}_{11} = i\mathbf{S}_{\chi} \cdot \mathbf{q}, \quad (47)$$

which generate a nuclear M response [26,28]. In this case, the generalized cross section reads

$$\begin{aligned} \frac{d\sigma_{\chi N}^{\text{SI}}}{d\mathbf{q}^2} &= \frac{\zeta^2}{4\pi\mathbf{v}^2} \left(\left| \sum_{I=\pm} [\xi_{\mathcal{O}_1} f_I^{\mathcal{O}_1}(\mathbf{q}^2) \mathcal{F}_I^M(\mathbf{q}^2) \right. \right. \\ &\quad \left. \left. + \xi_{\mathcal{O}_3} f_I^{\mathcal{O}_3}(\mathbf{q}^2) \mathcal{F}_I^{\Phi''}(\mathbf{q}^2)] \right. \right. \\ &\quad \left. \left. + \xi_{\pi} f_{\pi} \mathcal{F}_{\pi}(\mathbf{q}^2) + \xi_{\pi}^{\theta} f_{\pi}^{\theta} \mathcal{F}_{\pi}^{\theta}(\mathbf{q}^2) \right|^2 \right. \\ &\quad \left. + \sum_{i=5,8,11} \left| \sum_{I=\pm} \xi_{\mathcal{O}_i} f_I^{\mathcal{O}_i} \mathcal{F}_I^M(\mathbf{q}^2) \right|^2 \right). \quad (48) \end{aligned}$$

The separation into kinematics $\xi_{\mathcal{O}_i}$, nucleon form factors $f_{\pm}^{\mathcal{O}_i}$, and nuclear responses $\mathcal{F}(\mathbf{q}^2)$ is chosen in such a way that the form factors coincide with f_N and $f_1^{V,N}$ as defined in Secs. III B and III C. The form of the $\xi_{\mathcal{O}_i}$, which set the scale for the \mathcal{O}_5 , \mathcal{O}_8 , and \mathcal{O}_{11} contributions, originates in the NR expansion of the effective operator to which they first contribute: the vector-vector, axial-vector–vector, and pseudoscalar-scalar channels, respectively [37]

$$\begin{aligned} \mathcal{M}_{1,\text{NR}}^{VV}(\mathcal{O}_5) &= f_1^{V,N}(t) \frac{\mu_N}{m_N m_{\chi}} \mathcal{O}_5, \\ \mathcal{M}_{1,\text{NR}}^{AV}(\mathcal{O}_8) &= 2f_1^{V,N}(t) \mathcal{O}_8, \\ \mathcal{M}_{1,\text{NR}}^{PS}(\mathcal{O}_{11}) &= -f_N(t) \frac{1}{m_{\chi}} \mathcal{O}_{11}, \quad (49) \end{aligned}$$

together with the operator multipole decomposition [26,28]. Altogether this leads to

$$\begin{aligned} \xi_{\mathcal{O}_1} &= \xi_{\pi} = \xi_{\pi}^{\theta} = 1, \\ \xi_{\mathcal{O}_3} &= \frac{\mathbf{q}^2}{2m_N^2}, \\ \xi_{\mathcal{O}_5} &= \frac{\mu_N |\mathbf{q}| |\mathbf{v}_T^{\perp}|}{2m_{\chi} m_N}, \\ \xi_{\mathcal{O}_8} &= |\mathbf{v}_T^{\perp}|, \\ \xi_{\mathcal{O}_{11}} &= -\frac{|\mathbf{q}|}{2m_{\chi}}, \quad (50) \end{aligned}$$

with the corresponding form factors

$$\begin{aligned} f_{\pm}^{\mathcal{O}_1}(\mathbf{q}^2) &= f_{\pm}^M(\mathbf{q}^2), \\ f_{\pm}^{\mathcal{O}_3}(\mathbf{q}^2) &= f_{\pm}^{\Phi''}, \\ f_{\pm}^{\mathcal{O}_5} &= f_{\pm}^{\mathcal{O}_8} = \frac{1}{2} [f_1^{V,p} \pm f_1^{V,n}], \\ f_{\pm}^{\mathcal{O}_{11}} &= \frac{1}{2} [f_p \pm f_n], \quad (51) \end{aligned}$$

where for the operators in Eq. (47) only the leading term has been listed. The form factors for the $\mathcal{O}_{5,8,11}$ terms can be expressed in terms of the previously defined quantities f_N and $f_1^{V,N}$, since they first appear in the NR expansion of the effective operators in Eq. (13) with scalar and vector nucleon interactions, in a similar way as \mathcal{O}_1 and \mathcal{O}_3 .

We note that Eq. (48) shows that the $\mathcal{O}_{5,8,11}$ operators do not interfere with \mathcal{O}_1 or \mathcal{O}_3 [26,28]. This is because contrary to \mathcal{O}_1 and \mathcal{O}_3 , the operators \mathcal{O}_5 , \mathcal{O}_8 , and \mathcal{O}_{11} are linear in the WIMP spin \mathbf{S}_{χ} , and the corresponding interference terms vanish after averaging over WIMP spin projections. In addition, the kinematical factors imply that the contributions of $\mathcal{O}_{5,8,11}$ are suppressed by $|\mathbf{v}_T^{\perp}|$ or $1/m_{\chi}$. These two properties are crucial for the \mathcal{O}_3 operator being the main one-body correction to the standard SI analyses, as anticipated in Eq. (44). In Sec. IV we show this explicitly by studying the one-body structure factors for xenon isotopes.

IV. ONE-BODY CURRENTS

We calculate the structure factors as in our previous work [36,38,40], by performing large-scale shell-model calculations of all stable xenon isotopes in a valence space comprising the $0g_{7/2}$, $1d_{5/2}$, $1d_{3/2}$, $2s_{1/2}$, and $0h_{11/2}$ (nlj)

TABLE IV. Spin/parity J^Π of the nuclear ground states, harmonic-oscillator length b , and fit coefficients for the nuclear response functions \mathcal{F}_\pm^M and $\mathcal{F}_\pm^{\Phi'}$. The fit functions are $\mathcal{F}_\pm^M(u) = e^{-\frac{u}{2}} \sum_{i=0}^5 c_i^{M\pm} u^i$ (with $c_0 = A$ and $c_0 = Z - N$, respectively) and $\mathcal{F}_\pm^{\Phi'}(u) = e^{-\frac{u}{2}} \sum_{i=0}^4 c_i^{\Phi'\pm} u^i$, with $u = \mathbf{q}^2 b^2 / 2$. These forms correspond to the analytical solution in the harmonic-oscillator basis [91,92]. For the $L = 2$ multipoles in ^{131}Xe , see Table V.

Isotope	^{128}Xe	^{129}Xe	^{130}Xe	^{131}Xe	^{132}Xe	^{134}Xe	^{136}Xe
J^Π	0^+	$1/2^+$	0^+	$3/2^+$	0^+	0^+	0^+
b [fm]	2.2847	2.2873	2.2899	2.2925	2.2950	2.3001	2.3051
c_1^{M+}	-126.455	-128.09	-129.753	-131.26	-132.835	-135.861	-138.787
c_2^{M+}	35.82	36.4367	37.2381	37.8232	38.4665	39.6872	40.9048
c_3^{M+}	-3.669 91	-3.753 17	-3.892 91	-3.971 71	-4.069 99	-4.24713	-4.419 84
c_4^{M+}	0.125 062	0.129 553	0.139 778	0.142 995	0.149 636	0.159 053	0.165 388
c_5^{M+}	$-5.637 31 \times 10^{-4}$	$-6.558 16 \times 10^{-4}$	$-9.300 32 \times 10^{-4}$	$-9.129 55 \times 10^{-4}$	$-0.001 114 63$	$-0.001 257 24$	$-0.001 092 11$
c_1^{M-}	29.0588	30.6854	32.2019	33.7021	35.253	38.2701	41.2081
c_2^{M-}	-11.7104	-12.3687	-13.1152	-13.7433	-14.4437	-15.773	-17.0848
c_3^{M-}	1.684 47	1.779 28	1.907 75	2.000 31	2.113 05	2.320 61	2.526 35
c_4^{M-}	-0.082 004 4	-0.086 875 4	-0.094 818 4	-0.099 136 4	-0.105 689	-0.116 557	-0.126 86
c_5^{M-}	$6.657 81 \times 10^{-4}$	$7.394 74 \times 10^{-4}$	$8.479 75 \times 10^{-4}$	$8.606 86 \times 10^{-4}$	$9.613 44 \times 10^{-4}$	0.001 066 93	0.001 109 65
$c_0^{\Phi'+}$	-25.211	-26.1264	-27.7106	-28.0443	-28.7972	-29.5095	-29.8571
$c_1^{\Phi'+}$	17.592	18.4401	19.7108	20.0888	20.7751	21.5578	22.0402
$c_2^{\Phi'+}$	-3.464 66	-3.646 69	-3.858 05	-3.949 34	-4.0995	-4.273 08	-4.370 33
$c_3^{\Phi'+}$	0.224 722	0.239 379	0.252 667	0.260 624	0.272 865	0.287 393	0.296 134
$c_4^{\Phi'+}$	-0.003 5331 6	-0.003 997 79	-0.004 442 09	-0.004 688 46	-0.005 075 27	-0.005 554 37	-0.005 968 4
$c_0^{\Phi'-}$	3.896 29	5.470 22	6.285 19	6.905 42	7.931 45	9.3351	10.1433
$c_1^{\Phi'-}$	-4.731 63	-5.969 63	-6.638 42	-7.179 62	-8.010 86	-9.202 79	-9.961 23
$c_2^{\Phi'-}$	1.484 89	1.7533	1.854 06	1.972 17	2.128 17	2.354 89	2.487 84
$c_3^{\Phi'-}$	-0.140 203	-0.160 094	-0.166 079	-0.175 248	-0.186 148	-0.202 364	-0.212 062
$c_4^{\Phi'-}$	0.003 447 65	0.003 879 83	0.004 134 53	0.004 376 13	0.004 698 87	0.005 194 63	0.005 596 88

orbitals for both neutrons and protons, with n the radial quantum number, l the orbital angular momentum in spectroscopic notation, and j the total angular momentum. Our calculations therefore assume an isospin symmetric ^{100}Sn core. For ^{132}Xe , ^{134}Xe , and ^{136}Xe exact diagonalizations are obtained in this valence space, while for the remaining isotopes some truncations, which should not significantly affect the nuclear ground states, are needed to keep the matrix dimensions tractable, as discussed in Refs. [36,40]. We use the shell-model interaction GCN5082 [83,84], which has also been used in neutrinoless double-beta decay calculations of ^{136}Xe [83,84]. The low-energy excitation spectra of all isotopes are very well reproduced [36,40]. The nuclear-structure calculations have been performed with the shell-model code ANTOINE [85,86].

The phenomenological nature of the shell-model interaction used makes it difficult to estimate the theoretical uncertainties associated with the nuclear-structure calculations. Similarly, the systematic uncertainty due to the truncations needed for some isotopes is challenging to evaluate. It will be possible to address these aspects with calculations based on ChEFT interactions, which provide

natural diagnostics to estimate nuclear-structure uncertainties [87–90]. In the meantime, one measure for the reliability of the calculation can be obtained by comparing the predicted excitation spectra with the experimental results.

With the calculated xenon ground states we obtain all one-body nuclear responses needed in Eq. (44). The results, summarized in Tables IV and V, are presented in terms of the dimensionless parameter $u = \mathbf{q}^2 b^2 / 2$, where $b = \sqrt{\hbar / m_N \omega}$ is the harmonic-oscillator length and $\hbar \omega = (45A^{-1/3} - 25A^{-2/3})$ MeV. The nuclear response functions leading to the structure factors are fit to the form

$$\mathcal{F}(u) = e^{-\frac{u}{2}} \sum_{i=0}^m c_i u^i, \quad (52)$$

with $m = 5$ for \mathcal{F}_\pm^M , $m = 4$ for $\mathcal{F}_\pm^{\Phi'}$, and fixed coefficients $c_0 = A$ and $c_0 = Z - N$ for \mathcal{F}_\pm^M and $\mathcal{F}_\pm^{\Phi'}$, respectively. The form of the fit function follows the analytic solution of the transition operators evaluated in the harmonic-oscillator basis [91,92].

The isoscalar nuclear M operator has been known to lead to a coherent contribution from all nucleons for a long time (at zero momentum transfer) [22]. This justifies that the nuclear response \mathcal{F}_\pm^M associated with the \mathcal{O}_1 operator is the

TABLE V. Fit coefficients for the $L = 2$ multipoles in ^{131}Xe , parametrized by $\tilde{\mathcal{F}}_{\pm}^M(u) = e^{-\frac{u}{2}} \sum_{i=1}^5 \tilde{c}_i u^i$, $\tilde{\mathcal{F}}_{\pm}^{\Phi''}(u) = e^{-\frac{u}{2}} \sum_{i=0}^4 \tilde{c}_i u^i$. Notation and oscillator length are as in Table IV.

Response	\tilde{c}_1	\tilde{c}_2	\tilde{c}_3	\tilde{c}_4	\tilde{c}_5
$\tilde{\mathcal{F}}_+^M$	2.175 16	-1.253 86	0.214 567	-0.011 096 4	$7.990 74 \times 10^{-5}$
$\tilde{\mathcal{F}}_-^M$	-0.344 057	0.208 632	-0.048 112	0.003 515 88	$-8.145 09 \times 10^{-5}$
	\tilde{c}_0	\tilde{c}_1	\tilde{c}_2	\tilde{c}_3	\tilde{c}_4
$\tilde{\mathcal{F}}_+^{\Phi''}$	0.498 456	-0.028 914 9	-0.016 037 6	$-7.718 42 \times 10^{-5}$	$4.590 07 \times 10^{-4}$
$\tilde{\mathcal{F}}_-^{\Phi''}$	-0.751 871	1.068 26	-0.227 403	0.009 636 27	$-4.145 55 \times 10^{-4}$

only one considered in most SI dark-matter direct-detection analyses [2–10].

In turn, the nuclear Φ'' operator, at zero momentum transfer, is proportional to the sum over all nucleons of the single-nucleon spin-orbit ($\mathbf{l} \cdot \mathbf{s}$) operator [26,28]. This implies that nucleons in an orbital with spin parallel to the angular momentum, $j = l + 1/2$, contribute coherently. Similarly, the nucleons in the spin-orbit partner $j = l - 1/2$ also contribute coherently, in such a way that when both spin-orbit partners are filled their contributions exactly cancel. However, in heavy nuclei the spin-orbit splitting is important, with $j = l + 1/2$ orbitals having significantly lower energies than their spin-orbit partners. In the case of xenon isotopes this implies that the proton $0g_{9/2}$ and the neutron $0h_{11/2}$ orbitals are mostly filled (the latter especially for the more neutron-rich isotopes), with the spin-orbit partners, proton $0g_{7/2}$ and neutron $0h_{9/2}$ orbitals,

mostly empty. Therefore the nuclear Φ'' response, $\mathcal{F}^{\Phi''}$, shows a quasicohherent behavior [26,28], with the contributions of about 20 nucleons adding coherently in the isoscalar case. The total response is dominated by neutrons because the $l = 5$, $0h_{11/2}$ orbital accommodates 12 nucleons, compared to ten nucleons for the $l = 4$, $0g_{9/2}$ orbital (the expectation value of the single-particle spin-orbit operator is proportional to l for $j = l + 1/2$ orbitals). The nuclear response functions are larger for the most neutron-rich isotopes with more neutrons in the $0h_{11/2}$ orbital.

The quasicohherent nuclear response $\mathcal{F}^{\Phi''}$ is generated by the \mathcal{O}_3 operator. In addition, in the total structure factor there is an interference term between this contribution and the \mathcal{F}^M term from the dominant \mathcal{O}_1 operator, as indicated by Eq. (44) [26,28]. This interference is important because, as discussed in Sec. III D, there is no other interference term coming from one-body operators. Altogether, the nuclear response $\mathcal{F}^{\Phi''}$ generates the leading one-body-operator corrections to the structure factors usually considered in SI analyses.

This is illustrated in Figs. 3 and 4, which compare for the isoscalar and isovector cases, respectively, the structure factors associated with the coherent and quasicohherent nuclear M and Φ'' responses generated by the operators \mathcal{O}_1 , \mathcal{O}_3 , \mathcal{O}_{11} , \mathcal{O}_8 , and \mathcal{O}_5 . In this comparison the values of the associated nucleon couplings and form factors are not included, so some caution needs to be taken in the interpretation of the figures due to differences in the combination of the Wilson coefficients for the different contributions. However, the results are shown on a logarithmic scale, and the main features in Figs. 3 and 4 should still be valid once all corresponding couplings and form factors are included.

Figure 3 shows that the standard SI structure factor proportional to A^2 , originating from the \mathcal{O}_1 operator, receives the leading one-body correction from the interference with the $\mathcal{F}^{\Phi''}$ response due to \mathcal{O}_3 . This correction is only of the order of 1 per mil because $\mathcal{F}^{\Phi''}$ comes with a kinematical factor $\xi_{\mathcal{O}_3} = \mathbf{q}^2/2m_N^2$. Consequently, the interference term vanishes at $|\mathbf{q}| = 0$.

The next contribution in this hierarchy comes from the nuclear M response originating from the \mathcal{O}_{11} operator. Due

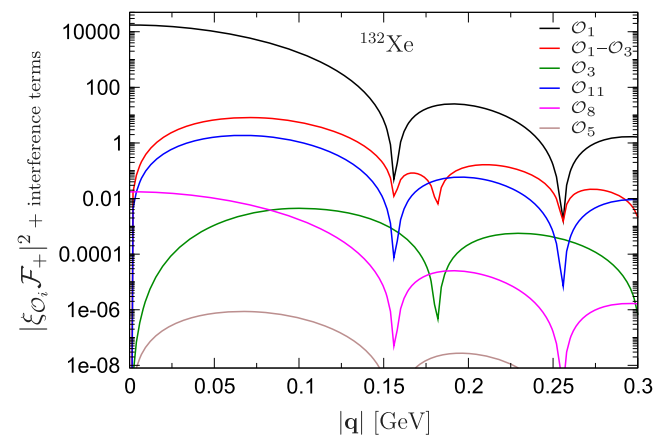


FIG. 3. Comparison of the isoscalar structure factors associated with the coherent and quasicohherent nuclear M and Φ'' responses. The individual contributions corresponding to the \mathcal{O}_1 , \mathcal{O}_3 , \mathcal{O}_{11} , \mathcal{O}_8 , and \mathcal{O}_5 operators, $|\xi_{\mathcal{O}_i} \mathcal{F}_+^{M/\Phi''}(\mathbf{q}^2)|^2$, and the absolute value of the \mathcal{O}_1 - \mathcal{O}_3 interference term, $|2\xi_{\mathcal{O}_1} \xi_{\mathcal{O}_3} \mathcal{F}_+^M(\mathbf{q}^2) \mathcal{F}_+^{\Phi''}(\mathbf{q}^2)|$, are shown. For the evaluation of the structure factors associated with \mathcal{O}_{11} , \mathcal{O}_8 , and \mathcal{O}_5 we take the relative WIMP velocity $|\mathbf{v}_T| = 10^{-3}$ and WIMP mass $m_\chi = 2$ GeV, roughly the minimal mass probed in xenon direct-detection experiments. The results, representative for all stable xenon isotopes, are shown for the most abundant ^{132}Xe .

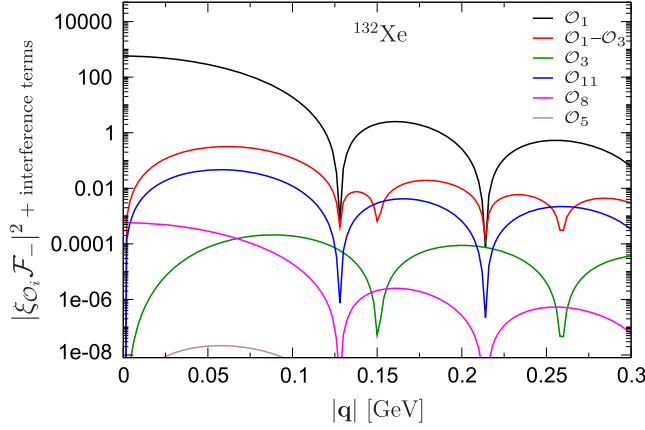


FIG. 4. Same as Fig. 3 but for the isovector case. The isovector individual structure factors $|\xi_{O_i} \mathcal{F}_{-}^{M/\Phi''}(\mathbf{q}^2)|^2$, and the absolute value of the \mathcal{O}_1 - \mathcal{O}_3 interference term $|2\xi_{O_1}\xi_{O_3}\mathcal{F}_{-}^{M}(\mathbf{q}^2)\mathcal{F}_{-}^{\Phi''}(\mathbf{q}^2)|$ are shown.

to the associated kinematical factor $\xi_{O_{11}} = |\mathbf{q}|/m_\chi$, this contribution also vanishes at $|\mathbf{q}| = 0$, and becomes less important for heavier WIMPs. Figure 3 shows the results for $m_\chi = 2$ GeV, roughly the smallest WIMP mass probed by xenon direct-detection experiments. For heavier WIMPs the structure factor associated with the \mathcal{O}_{11} operator is reduced, and for $m_\chi \approx 50$ GeV this structure factor is comparable to the one corresponding to the \mathcal{O}_3 operator, originating solely from the nuclear $\mathcal{F}^{\Phi''}$ response. The latter structure factor is suppressed by 3 additional orders of magnitude compared to the leading correction to the standard SI structure factor, the \mathcal{O}_1 - \mathcal{O}_3 interference term.

Finally, the structure factors coming from the nuclear M responses associated with the \mathcal{O}_8 and \mathcal{O}_5 operators are even smaller, because they are suppressed by the very small WIMP velocity $|\mathbf{v}_T^\perp| \approx 10^{-3}$ in their kinematical factors, see Eq. (50). Note that, as emphasized in Refs. [26,28], the \mathcal{O}_3 operator, similarly to \mathcal{O}_8 and \mathcal{O}_5 , involves the velocity operator \mathbf{v}^\perp , but for \mathcal{O}_3 the associated nuclear operator does not depend on the WIMP velocity with respect to the center of mass, \mathbf{v}_T^\perp , but on the nucleon's velocity operator, which is part of the Φ'' operator and generates a milder suppression factor $|\mathbf{q}|/m_N$.

The isovector results shown in Fig. 4 are very similar to the isoscalar case. The only difference is that all structure factors are smaller because in this case the contributions of protons and neutrons partially cancel.

Similarly to this generalized SI analysis, the standard SD structure factor will receive additional contributions beyond the \mathcal{O}_4 and \mathcal{O}_6 operators. In particular, the \mathcal{O}_3 , \mathcal{O}_7 , \mathcal{O}_9 , and \mathcal{O}_{10} operators contribute to Σ' or Σ'' , and \mathcal{O}_5 , \mathcal{O}_8 to the additional Δ response. In addition there will be \mathcal{O}_4 - \mathcal{O}_5 and \mathcal{O}_8 - \mathcal{O}_9 Σ' - Δ interference terms [26]. All these additional contributions vanish at $|\mathbf{q}| = 0$, except for the \mathcal{O}_7 response which is suppressed by the WIMP velocity

$|\mathbf{v}_T^\perp| \approx 10^{-3}$. Note also that only \mathcal{O}_5 interferes with the dominant SD response, but this operator only appears at higher (fourth) order in ChEFT [37]. Likewise, the $\tilde{\Phi}'$ response receives contributions from higher ChEFT orders only. Therefore these corrections to SD scattering are expected to be small. We defer a detailed analysis of generalized SD scattering to future work.

V. TWO-BODY CURRENTS

As discussed in Sec. IV the shell-model calculations are based on a core, while the many-body problem is explicitly solved for nucleons close to the Fermi level in the valence space. This generally leads to very good agreement to experiment for spectroscopy [86], including the isotopes relevant for dark-matter direct detection [38,40].

However, for the standard SI scattering (nuclear M response) all nucleons contribute coherently, so that the bulk of the nuclear response is in fact generated by the inert core. A similar argument can be made for the quasicohherent Φ'' response in xenon, where the core protons in the $0g_{9/2}$ orbital are responsible for about half of the total response. The relatively small sensitivity of these nuclear responses to the nuclear structure was discussed in Ref. [40], and justifies the use of the simple Helm form factor [see Eq. (12)] in the standard SI analysis.

In addition, the nuclear response can be calculated in a noninteracting shell-model picture, where only the lowest-lying orbitals are filled with particles. Figure 5 shows the $\mathcal{F}_+^M(\mathbf{q}^2)$ response for ^{129}Xe , using a noninteracting shell model and single-particle orbitals with and without j -coupling (but with occupation numbers from the interacting shell model, see Table VI). The agreement with the full shell-model calculation is very good, showing that the dependence on correlations among the valence nucleons as

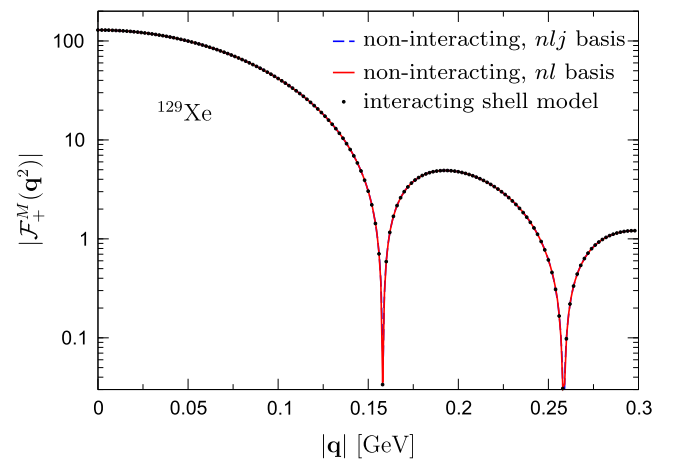


FIG. 5. $\mathcal{F}_+^M(\mathbf{q}^2)$ for ^{129}Xe obtained from three different approximations: shell-model calculation from [40] (black dots), noninteracting shell model with j -coupling (red solid line), and in nl basis (blue dashed line).

TABLE VI. Relative occupation numbers n_{nl}^r for the nl orbitals in ^{129}Xe and maximum occupation including spin degeneracy. For orbitals in the valence space, the results of the shell-model diagonalization are used.

n	l	Maximum occupation	n_{nl}^p	n_{nl}^n
0	0	2	1	1
0	1	6	1	1
0	2	10	1	1
1	0	2	1	1
0	3	14	1	1
1	1	6	1	1
0	4	18	0.68	0.99
1	2	10	0.16	0.79
2	0	2	0.06	0.58
0	5	22	0.01	0.37

well as j -coupling effects are small for this response. Likewise, the effect of using naive or shell-model-based occupation numbers would be hardly visible in the figure.

In view of these findings, we evaluate the two-body matrix elements of Eq. (38) by

$$\mathcal{F}_\pi(\mathbf{q}^2) = \frac{1}{2} \sum_{\text{occ}} \langle N_1 N_2 | (1 - P_{12}) | \frac{1}{f_\pi} \mathcal{M}_{2,\text{NR}}^{SS} | N_1 N_2 \rangle, \quad (53)$$

$$|N_1 N_2\rangle = |n_1 l_1 m_1 \sigma_1 \tau_1 n_2 l_2 m_2 \sigma_2 \tau_2\rangle,$$

and analogously for $\mathcal{F}_\pi^\theta(\mathbf{q}^2)$, where the sum runs over occupied states (e.g., for ^{129}Xe according to Table VI) and $P_{12} = P_k P_\sigma P_\tau$ is the exchange operator with

$$P_\sigma = \frac{1}{2} (\mathbb{1} + \boldsymbol{\sigma}_1 \cdot \boldsymbol{\sigma}_2), \quad P_\tau = \frac{1}{2} (\mathbb{1} + \boldsymbol{\tau}_1 \cdot \boldsymbol{\tau}_2), \quad (54)$$

TABLE VII. Spin/parity J^Π of the nuclear ground states, harmonic-oscillator length b , and fit coefficients for the nuclear response functions \mathcal{F}_π and \mathcal{F}_π^θ , with fit functions $\mathcal{F}_\pi(u) = e^{-\frac{u}{2}} \sum_{i=0}^5 c_i^\pi u^i$, $\mathcal{F}_\pi^\theta(u) = e^{-\frac{u}{2}} \sum_{i=0}^5 c_i^\theta u^i$, and $u = \mathbf{q}^2 b^2 / 2$.

Isotope	^{128}Xe	^{129}Xe	^{130}Xe	^{131}Xe	^{132}Xe	^{134}Xe	^{136}Xe
J^Π	0^+	$1/2^+$	0^+	$3/2^+$	0^+	0^+	0^+
b [fm]	2.2847	2.2873	2.2899	2.2925	2.2950	2.3001	2.3051
c_0^π	-2.42605	-2.44233	-2.45715	-2.47546	-2.49308	-2.52965	-2.56752
c_1^π	2.018 83	2.036 93	2.063	2.086 43	2.110 87	2.155 56	2.196 45
c_2^π	-0.576294	-0.579809	-0.594377	-0.602812	-0.612728	-0.62789	-0.642445
c_3^π	0.077 613	0.077 520 1	0.081 030 7	0.082 407 2	0.084 465 2	0.086 328 8	0.088 341 1
c_4^π	-0.00519097	-0.00512894	-0.0055788	-0.00570646	-0.00597987	-0.00602651	-0.00611004
c_5^π	$1.390 81 \times 10^{-4}$	$1.353 27 \times 10^{-4}$	$1.592 49 \times 10^{-4}$	$1.653 35 \times 10^{-4}$	$1.821 98 \times 10^{-4}$	$1.780 02 \times 10^{-4}$	$1.750 76 \times 10^{-4}$
c_0^θ	-24.876 8	-25.039	-25.2034	-25.3895	-25.5691	-25.9446	-26.3396
c_1^θ	18.5427	18.8087	18.9813	19.2032	19.4359	19.8659	20.248
c_2^θ	-4.815 14	-4.901 61	-4.967 98	-5.035 73	-5.115 92	-5.2492	-5.383 23
c_3^θ	0.631 787	0.644 029	0.650 297	0.658 108	0.670 645	0.683 946	0.707 54
c_4^θ	-0.047 776 1	-0.048 890 6	-0.048 337 7	-0.048 736 2	-0.050 024 3	-0.049 659	-0.052 296 9
c_5^θ	0.001 714 69	0.001 772 9	0.001 658 85	0.001 673 17	0.001 747 03	0.001 635 41	0.001 781

and P_k exchanges the momenta. Summing over spins σ_i and evaluating the matrix element in Eq. (53) in the harmonic-oscillator basis, we obtain

$$\mathcal{F}_\pi(\mathbf{q}^2) = \frac{M_\pi}{2} \left(\frac{g_A}{2F_\pi} \right)^2 \sum_{n_1 l_1 n_2 l_2} \sum_{\tau_1 \tau_2} \int \frac{d^3 p_1 d^3 p_2 d^3 p'_1 d^3 p'_2}{(2\pi)^6} \times R_{n_1 l_1}(|\mathbf{p}'_1|) R_{n_2 l_2}(|\mathbf{p}'_2|) R_{n_1 l_1}(|\mathbf{p}_1|) R_{n_2 l_2}(|\mathbf{p}_2|) \times \frac{(2l_1 + 1)(2l_2 + 1)}{16\pi^2} P_{l_1}(\hat{\mathbf{p}}'_1 \cdot \hat{\mathbf{p}}_1) P_{l_2}(\hat{\mathbf{p}}'_2 \cdot \hat{\mathbf{p}}_2) \times (2\pi)^3 \delta^{(3)}(\mathbf{p}_1 + \mathbf{p}_2 - \mathbf{p}'_1 - \mathbf{p}'_2 - \mathbf{q}) \times (3 - \boldsymbol{\tau}_1 \cdot \boldsymbol{\tau}_2) \frac{\mathbf{q}_1^{\text{ex}} \cdot \mathbf{q}_2^{\text{ex}}}{((\mathbf{q}_1^{\text{ex}})^2 + M_\pi^2)((\mathbf{q}_2^{\text{ex}})^2 + M_\pi^2)}, \quad (55)$$

with

$$\mathbf{q}_1^{\text{ex}} = \mathbf{p}'_2 - \mathbf{p}_1, \quad \mathbf{q}_2^{\text{ex}} = \mathbf{p}'_1 - \mathbf{p}_2, \quad \mathbf{q} = -\mathbf{q}_1^{\text{ex}} - \mathbf{q}_2^{\text{ex}}, \quad (56)$$

and radial wave functions

$$R_{nl}(k) = b^{3/2} \sqrt{\frac{2n!}{\Gamma(n+l+3/2)}} (bk)^l e^{-\frac{(bk)^2}{2}} L_n^{l+1/2}[(bk)^2]. \quad (57)$$

The expression for $\mathcal{F}_\pi^\theta(\mathbf{q}^2)$ is analogous. The sum over m_1, m_2 has been performed using the addition theorem for the spherical harmonics, assuming an equal filling of all orbitals with different m projections. Apart from the momentum integrals, which can be performed numerically for given $\{n_1 l_1 n_2 l_2\}$, only the isospin part of Eq. (55) needs to be evaluated. This leads to

$$\sum_{n_1 l_1 n_2 l_2} \sum_{\tau_1 \tau_2} (3 - \tau_1 \cdot \tau_2) = 2 \sum_{n_1 l_1 n_2 l_2} [n_{n_1 l_1}^p n_{n_2 l_2}^p + n_{n_1 l_1}^n n_{n_2 l_2}^n + 4n_{n_1 l_1}^p n_{n_2 l_2}^n], \quad (58)$$

where the n_{nl}^r denote the relative occupation numbers of a given orbital. In Table VI we list these occupation numbers for the case of ^{129}Xe used in the calculation of \mathcal{F}_π and \mathcal{F}_π^θ as well as the nl -basis calculation shown in Fig. 5. For orbitals in the valence space of the shell-model calculations, the result of the full diagonalization is used, even though the sensitivity to this is minor.

The results for \mathcal{F}_π and \mathcal{F}_π^θ can be fit with the same functional form as given in Eq. (52) for the one-body case, see Table VII for the corresponding coefficients. Keeping terms up to $m = 5$ provides the best description also for the two-body terms. This form can be expected based on normal-ordering arguments: after the summation over the second nucleon, the result only depends on \mathbf{p}_1 , \mathbf{p}'_1 , and $\boldsymbol{\sigma}_1$, so that the corresponding operators depend on \mathbf{q} , \mathbf{v}^\perp , and \mathbf{S}_N , and can be written in terms of \mathcal{O}_1 , \mathcal{O}_3 , as well as other operators subleading in our analysis. Then the summation over spins performed before Eq. (55) eliminates the dependence on \mathcal{O}_3 (as well as higher multipoles). Therefore, apart from suppressed contributions, we expect the normal ordering to reduce the two-body matrix element to a one-body matrix element of \mathcal{O}_1 , with corresponding fit function as given in Eq. (52) with $m = 5$.

We note that the equal-filling approximation picks out the $L = 0$ part of the response, as required for the decomposition of the SI structure factor given in Eq. (44). The $L = 2$ multipole contribution, only relevant for ^{131}Xe , would only appear as a correction to the strongly suppressed one-body $L = 2$ structure factor, which itself enters below the \mathcal{O}_{11} curve in Fig. 3. Therefore it can be safely neglected.

The $\mathcal{F}_\pi(0)$ contribution has been considered before in Refs. [34,35,39], based on results for closed-shell nuclei and represented in terms of a fit linear in A . In our conventions, the results for $A = 132$ are $\mathcal{F}_\pi(0) = -2.4(0.8)$ [34], $\mathcal{F}_\pi(0) = -1.4$ [35], and $\mathcal{F}_\pi(0) = -1.9$ [39], in reasonable agreement with our value. The remaining differences can be traced back to our improved nuclear structure calculation and additional corrections from modeling nuclear short-range correlations [93] included in Refs. [34,35,39]. The latter are not dictated by ChEFT in this form, and thus not present in our calculation. This strategy is in agreement with findings for nuclear matrix elements of neutrinoless double-beta decay [94,95], where the effects of short-range correlations are small after the momentum dependence of the one-body currents is included.

The consequences for the structure factors are illustrated in Fig. 6, an extension of Fig. 3 that includes the effect of $\mathcal{F}_\pi(\mathbf{q}^2)$ and $\mathcal{F}_\pi^\theta(\mathbf{q}^2)$ as well as the interference terms with

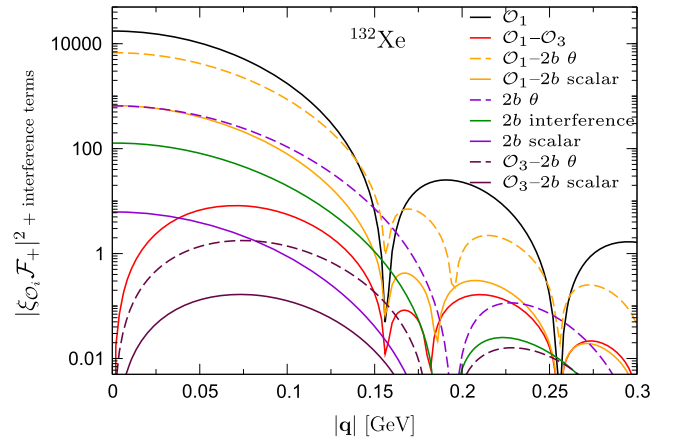


FIG. 6. Same as Fig. 3, but including the two-body-current contribution $|\xi_\pi^{(\theta)} \mathcal{F}_\pi^{(\theta)}(\mathbf{q}^2)|^2$ as well as the interference terms $|2\xi_{\mathcal{O}_1} \xi_\pi^{(\theta)} \mathcal{F}_+^M(\mathbf{q}^2) \mathcal{F}_\pi^{(\theta)}(\mathbf{q}^2)|$ and $|2\xi_{\mathcal{O}_3} \xi_\pi^{(\theta)} \mathcal{F}_+^{\Phi'}(\mathbf{q}^2) \mathcal{F}_\pi^{(\theta)}(\mathbf{q}^2)|$. Solid (dashed) lines refer to \mathcal{F}_π (\mathcal{F}_π^θ). The green line indicates the interference $|2\xi_\pi \xi_\pi^\theta \mathcal{F}_\pi(\mathbf{q}^2) \mathcal{F}_\pi^\theta(\mathbf{q}^2)|$ of the two-body terms. The responses associated with \mathcal{O}_3 , \mathcal{O}_5 , \mathcal{O}_8 , and \mathcal{O}_{11} have been omitted for clarity.

the isoscalar one-body operators. Figure 6 shows that the two-body contributions constitute the leading correction to the \mathcal{O}_1 structure factor. In particular, $\mathcal{F}_\pi^\theta(0)$ surpasses $\mathcal{F}_\pi(0)$ by an order of magnitude, to end up at a similar level as the isovector one-body contribution. Equation (38) illustrates the reason for this enhancement: the factor 4 from the momentum-independent term and the fact that the integral over $-\mathbf{q}_1 \cdot \mathbf{q}_2 / M_\pi^2$ adds an additional factor about 3 combine to the final factor of 10. It is also important to note that, in contrast to the structure factor associated with \mathcal{O}_3 (including its interference with \mathcal{O}_1) the two-body structure factors do not vanish at $|\mathbf{q}| = 0$.

Even though the main hierarchy suggested by Fig. 6 should be relatively general, we stress that this comparison assumes that the nucleon form factors are all of roughly the same size, and that additional relative suppressions and enhancements may occur, as for instance indicated by the simple models explored in Sec. VIC, where the relative size of both two-body terms is seen to be similar due to the large single-nucleon matrix element that compensates for the larger $\mathcal{F}_\pi^\theta(0)$.

Also, when comparing the hierarchy of isoscalar and isovector responses, one should keep in mind that for theories with an approximate isospin symmetry, there could be an additional suppression hidden, e.g., in $f_p - f_n$. In either case, the dominant contribution will actually be generated by the interference term $|2\mathcal{F}_+^M(\mathbf{q}^2) \mathcal{F}_-^M(\mathbf{q}^2)|$ with the isoscalar response. In addition to the hierarchies studied in Figs. 3, 4, and 6, there are also \mathbf{q}^2 -dependent corrections to the one-body form factors, which we address in the following section.

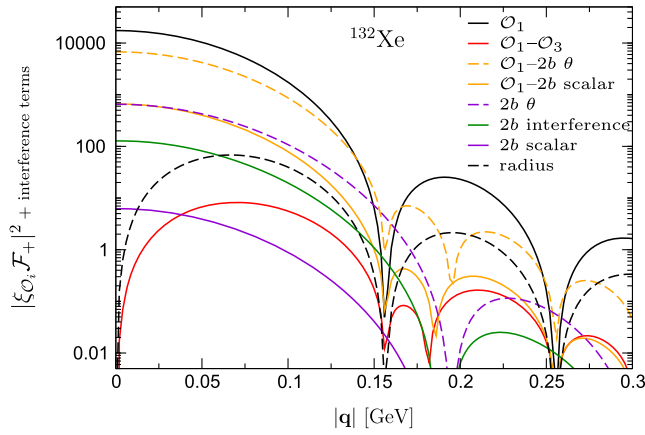


FIG. 7. Same as Fig. 6, but including the generic size of radius corrections (black dashed line), as discussed in the text. Note that the \mathcal{O}_3 - $2b$ interference terms have been dropped.

VI. PARAMETERS IN GENERAL SPIN-INDEPENDENT SCATTERING

The hierarchy of the one- and two-body contributions discussed in Secs. IV and V, combined with the general expression for the structure factor in Eq. (44), determines the number of independent parameters in our analysis of general SI scattering. First, however, we need to quantify the momentum-dependent corrections to the one-body form factors reviewed in Secs. III B and III C, including the scalar radii, anomalous magnetic moments, as well as strangeness radii and moments. We refer generically to all these contributions as radius corrections. They are evaluated in Sec. VI A. In Sec. VI B we then discuss the number of independent parameters appearing in the analysis of general SI scattering, and as examples, in Sec. VI C we focus on two simple cases: the case of scalar interactions with u and d quarks only, and purely gluonic couplings.

A. Radius corrections

The chiral counting that underlies the decomposition in Eqs. (44) and (45) implies that radius corrections are expected to contribute at a similar level as the leading two-body currents. Moreover, since only the coefficients of $\mathcal{F}_\pm^M(\mathbf{q}^2)$ are affected, these corrections concern the response of the \mathcal{O}_1 operator, being coherently enhanced. By definition, radius corrections vanish for vanishing momentum transfer, but they could become relevant for larger \mathbf{q}^2 values. The exact shape depends on the underlying BSM physics as well as on their relative size compared to the leading nucleon form factor, e.g., as seen in Eq. (31), in the case of C_s^{VV} the leading contribution vanishes and radius corrections generate all sensitivity to this Wilson coefficient.

In order to estimate the generic size of radius corrections in a simple way, we factor out the nucleon mass as a

representative hadronic scale, leading to a typical \mathbf{q}^2/m_N^2 suppression in the associated structure factor. This is illustrated in Fig. 7 by means of the interference term of radius corrections with \mathcal{O}_1 (again assuming that the remaining coefficients are both equal to 1). As expected, the correction is irrelevant at $|\mathbf{q}| = 0$, but it is one of the largest contributions for finite $|\mathbf{q}|$, only second to the \mathcal{O}_1 -two-body interference and $|\mathcal{F}_\pi^\theta|^2$ (and thus also below the interference with the isovector \mathcal{O}_1 operator not shown in Fig. 7). In particular Fig. 7 shows that the radius corrections are expected to be more important than the interference of the standard SI response with the new NREFT operator \mathcal{O}_3 . This estimate supports the expectation from ChEFT that radius corrections need to be included on the same footing as higher-order momentum-dependent operators.

B. Independent parameters

Within the formalism put forward in Sec. III, the decomposition of the WIMP-nucleus cross section in Eq. (44) therefore involves eight parameters that can be extracted from the dependence on Z , N , and $|\mathbf{q}|$, i.e., from direct-detection measurement on different nuclear targets. These are

- (1) two (isoscalar and isovector) leading coefficients of the M response

$$c_\pm^M = \frac{\zeta}{2} [f_p \pm f_n + f_1^{V,p} \pm f_1^{V,n}], \quad (59)$$

- (2) two coefficients of the two-body responses

$$c_\pi = \zeta f_\pi, \quad c_\pi^\theta = \zeta f_\pi^\theta, \quad (60)$$

- (3) two (isoscalar and isovector) radius corrections to the M response

$$\begin{aligned} \dot{c}_\pm^M = & \frac{\zeta m_N^2}{2} \left[\dot{f}_p \pm \dot{f}_n + \dot{f}_1^{V,p} \pm \dot{f}_1^{V,n} \right. \\ & \left. + \frac{1}{4m_N^2} (f_2^{V,p} \pm f_2^{V,n}) \right], \end{aligned} \quad (61)$$

- (3) two (isoscalar and isovector) coefficients of the Φ'' response

$$c_\pm^{\Phi''} = \frac{\zeta}{2} (f_2^{V,p} \pm f_2^{V,n}). \quad (62)$$

These eight parameters are not all independent, since they map onto the seven Wilson coefficients C_q^{SS} , C_g^{SS} , and C_q^{VV} (with $q = u, d, s$) for a Dirac WIMP, which reduces to four in the Majorana case where the C_q^{VV} vanish. Indeed, if

higher orders in the momentum expansion or η -exchange currents were considered, the number of parameters in the decomposition of the nucleon form factors and two-body currents would be even larger, so that in general a correlated analysis is called for.

The discussion of hierarchies in terms of Figs. 3, 4, 6, and 7 also shows that if the minimal extension of the standard SI response is sought, the analysis should include c_{\pm}^M , c_{π} , and c_{π}^{θ} , extending the standard formalism by the leading isovector and two-body responses. These findings provide the basis for the discussion of the general SI analysis strategy for direct-detection experiments formulated in Sec. II.

C. Examples: Scalar interactions with u and d quarks and purely gluonic couplings

Further simplifications can occur if specific assumptions are made about the Wilson coefficients. As an example, we first consider the case of purely scalar interactions, $C_q^{VV} = 0$, with u and d quarks only, i.e., with $C_s^{SS} = C_g^{SS} = 0$. In this case, the nonvanishing hadronic coefficients in Eq. (45) become related according to

$$\begin{aligned} \frac{f_p + f_n}{2} &= \frac{\sigma_{\pi N}}{M_{\pi}} f_{\pi} = 0.43(3) f_{\pi}, \\ \frac{f_p - f_n}{2} &= -\frac{2Bc_5(m_d - m_u)}{\xi M_{\pi}} \tilde{f}_{\pi} = 0.020(5) \tilde{f}_{\pi}, \\ \frac{\dot{f}_p + \dot{f}_n}{2} &= \frac{\dot{\sigma}}{M_{\pi}} f_{\pi} = 1.72(6) m_N^{-2} f_{\pi}. \end{aligned} \quad (63)$$

Therefore, there are only two linearly independent parameters, namely the isoscalar and the isovector coupling to the nucleon ($f_p \pm f_n$ or equivalently f_{π} and \tilde{f}_{π}); the other parameters, the coupling to the pion and the nucleon radius corrections are then fully determined. To calculate the coefficients in the above equations, we have used $\sigma_{\pi N} = 59.1(3.5)$ MeV from Ref. [55], $\dot{\sigma}$ and ξ as given in Sec. III B, and $Bc_5(m_d - m_u) = -0.51(8)$ MeV as extracted from the electromagnetic proton-neutron mass difference $(m_p - m_n)^{\text{em}} = 0.76(30)$ MeV via the Cottingham formula [96–98] (and consistent with lattice determinations [99]). The new hadronic coefficient (in addition to the standard SI analysis) is then given by

$$\tilde{f}_{\pi} = \frac{M_{\pi}}{\Lambda^3} (C_u^{SS} f_u^{\pi} - C_d^{SS} f_d^{\pi}), \quad (64)$$

thus differing by the relative sign from f_{π} [see Eq. (27)]. According to Eq. (63), the isoscalar hadronic form factor and its radius correction are of the same size as the two-body coefficient f_{π} up to a factor of 2, while the isovector contribution is further suppressed by an order of magnitude (the size of such isospin-violating effects has been studied

in the context of simplified models in Ref. [100]), unless this suppression in the hadronic input is balanced by \tilde{f}_{π}/f_{π} .

At $|\mathbf{q}| = 0$, the dominant correction to the standard SI response is thus generated by the two-body current, a reduction of the WIMP-nucleon cross section by about³

$$2 \frac{2f_{\pi}}{f_p + f_n} \frac{\mathcal{F}_{\pi}(0)}{A} = -9\%, \quad (65)$$

followed by the isovector contribution, which affects the rate by

$$2 \frac{f_p - f_n}{f_p + f_n} \frac{Z - N}{A} = -2\% \frac{\tilde{f}_{\pi}}{f_{\pi}}. \quad (66)$$

As a second example, it is also instructive to consider the case of purely gluonic interactions, i.e., all Wilson coefficients equal to zero apart from C_g^S . In this case the relative size of two-body contributions becomes

$$\begin{aligned} &2 \frac{f_{\pi} \mathcal{F}_{\pi}(0) + f_{\pi}^{\theta} \mathcal{F}_{\pi}^{\theta}(0)}{f_N A} \\ &= -2 \frac{M_{\pi}}{m_N} \frac{2}{27 f_Q^N} \frac{\mathcal{F}_{\pi}(0) - \mathcal{F}_{\pi}^{\theta}(0)}{A} = -6\%, \end{aligned} \quad (67)$$

where the large numerical value of $\mathcal{F}_{\pi}^{\theta}(0)$ balances the large coupling of the nucleon to the gluon operator to produce an effect of similar magnitude as in Eq. (65).

These examples demonstrate that the hierarchy implied by the nuclear structure factors themselves can be upset if enhancements or suppressions in the coefficients, either the nucleon matrix elements or the Wilson coefficients, are present: in a similar way as $\mathcal{F}_{\pi}^{\theta}$ appears enhanced compared to the scalar two-body response \mathcal{F}_{π} , but is compensated by a large nucleon matrix element, the impact of the isovector one-body response is suppressed by small isospin-breaking effects in the nucleon couplings, see Eq. (63).

While the size of two-body corrections can be enhanced by fine-tuning the one-body coefficients (the one-response-at-a-time strategy put forward in Sec. II corresponds to the case where the cancellation is complete), the special cases in Eqs. (65)–(67) indicate the size of effects to be expected in regions of parameter space where no such cancellations of the leading contributions occur.

We stress that in the general case no interrelations such as Eqs. (65) or (67) between the different form factors exist, except for those dictated by QCD, e.g. $f_2^{V,N}$ contributing both

³The very large effects of up to 60% quoted in Ref. [34] rely on a specific parameter choice $r \approx 1$. For the example considered here, this implies $2f_{\pi}/(f_p + f_n) \approx M_{\pi}/(m_u + m_d) \approx 17$, in contradiction to Eq. (63). For realistic values of the hadronic couplings the two-body corrections are of the expected size of 5%–10%, while enhancements are possible if cancellations in the leading contribution occur.

to $\mathcal{F}_{\pm}^{\Phi'}$ and to the radius correction to \mathcal{F}_{\pm}^M . Even in the very special case of scalar interactions considered in Eq. (63) the dependence on the Wilson coefficients fully factorizes only if $f_{\pi} = \tilde{f}_{\pi}$ is assumed, or if the isovector contribution is neglected. In these extreme cases the limits on the scattering rate immediately translate to a limit on the single parameter f_{π} and thereby a fixed combination of C_u^{SS} and C_d^{SS} .

In general, direct-detection experiments are sensitive to several independent combinations of Wilson coefficients, whose determination therefore requires a correlated analysis of different targets. Otherwise, simplified strategies such as constraining one response at a time amount to considering slices through the parameter space of Wilson coefficients at the hadronic scale. This information can then be transferred to a given new-physics model, keeping in mind the operator running and mixing to be applied when translating the limits to BSM scales [46,101–104]. In the interpretation of such limits one also needs to take into account that not all coefficients are necessarily independent, e.g., for the spin-1/2 case considered in this paper eight parameters map onto only seven (four) Wilson coefficients in the Dirac (Majorana) case.

VII. SUMMARY

We have presented a strategy for the analysis of general SI WIMP scattering off nuclei, keeping all terms that lead to a coherent contribution of nucleons in nuclei and appear up to third order in the power counting of the WIMP-nucleon interaction according to ChEFT. Up to dimension 7 in an effective Lagrangian for WIMP and Standard-Model fields, scalar and vector interactions on the nucleon side can give rise to coherent enhancements. Our analysis shows that the leading corrections to the standard SI response are the isovector counterpart and the coherent contribution of WIMPs interacting with two nucleons (two-body currents). For a more detailed analysis, the next corrections to be included are momentum-dependent corrections to the

nucleon form factors as well as the quasicohherent response associated with the nucleon spin-orbit operator. The latter only contributes in the case of vector interactions. Therefore, it could potentially be used as a tool to experimentally discriminate between the scalar and vector channels.

Overall, we have found that a generalized SI scattering cross section including the dominant coherent corrections depends on eight parameters (four in a minimal extension), which in principle can be fixed by experiments performed with different nuclear targets, and we have discussed how to constrain these parameters in direct-detection experiments. For the case of WIMPs scattering off xenon isotopes, we have provided parametrizations of all relevant one- and two-body nuclear responses based on state-of-the-art nuclear shell-model calculations. These can be directly used for a general SI analysis of direct-detection experiments, considering, e.g., one response function at a time. In particular, our results show that direct-detection experiments are sensitive to additional BSM physics than the one coupling constrained in present standard SI analyses, and thus impose additional restrictions on the parameter space of a given new-physics model.

ACKNOWLEDGMENTS

We thank Laura Baudis, Silas R. Beane, Vincenzo Cirigliano, Michael L. Graesser, Richard J. Hill, Martin J. Savage, and Mikhail P. Solon for helpful discussions. This work was supported in part by the U.S. DOE Grant No. DE-FG02-00ER41132, the ERC Grant No. 307986 STRONGINT, the DFG through Grant No. SFB 1245, the Max-Planck Society, and JSPS Grant-in-Aid for Scientific Research No. 26-04323. J.M. was supported by an International Research Fellowship from JSPS. We thank the Institute for Nuclear Theory at the University of Washington for its hospitality and the U.S. DOE for partial support during the completion of this work.

-
- [1] L. Baudis, *J. Phys. G* **43**, 044001 (2016).
 - [2] E. Aprile *et al.* (XENON100 Collaboration), *Phys. Rev. Lett.* **109**, 181301 (2012).
 - [3] R. Agnese *et al.* (SuperCDMS Collaboration), *Phys. Rev. Lett.* **112**, 241302 (2014).
 - [4] R. Agnese *et al.* (SuperCDMS Collaboration), *Phys. Rev. Lett.* **116**, 071301 (2016).
 - [5] D. S. Akerib *et al.* (LUX Collaboration), *Phys. Rev. Lett.* **116**, 161301 (2016).
 - [6] X. Xiao *et al.* (PandaX Collaboration), *Phys. Rev. D* **92**, 052004 (2015).
 - [7] G. Angloher *et al.* (CRESST Collaboration), *Eur. Phys. J. C* **76**, 25 (2016).
 - [8] C. Amole *et al.* (PICO Collaboration), *Phys. Rev. D* **93**, 061101 (2016).
 - [9] P. Agnes *et al.* (DarkSide Collaboration), *Phys. Rev. D* **93**, 081101 (2016).
 - [10] E. Armengaud *et al.* (EDELWEISS Collaboration), *J. Cosmol. Astropart. Phys.* **05** (2016) 019.
 - [11] E. Aprile *et al.* (XENON Collaboration), *J. Cosmol. Astropart. Phys.* **04** (2016) 027.
 - [12] M. G. Boulay (DEAP Collaboration), *J. Phys. Conf. Ser.* **375**, 012027 (2012).
 - [13] J. Calvo *et al.* (ArDM Collaboration), [arXiv:1505.02443](https://arxiv.org/abs/1505.02443).
 - [14] D. S. Akerib *et al.* (LZ Collaboration), [arXiv:1509.02910](https://arxiv.org/abs/1509.02910).

- [15] E. Aprile *et al.* (XENON1T Collaboration), *J. Instrum.* **9**, P11006 (2014).
- [16] J. Liu (XMASS Collaboration), *AIP Conf. Proc.* **1604**, 397 (2014).
- [17] P. Agnes *et al.* (DarkSide project Collaboration), *J. Instrum.* **11**, C02051 (2016).
- [18] J. Aalbers *et al.*, [arXiv:1606.07001](https://arxiv.org/abs/1606.07001).
- [19] P. L. Brink (SuperCDMS Collaboration), *J. Low Temp. Phys.* **167**, 1093 (2012).
- [20] A. E. Chavarria *et al.*, *Phys. Procedia* **61**, 21 (2015).
- [21] G. Angloher *et al.* (CRESST Collaboration), [arXiv:1503.08065](https://arxiv.org/abs/1503.08065).
- [22] J. Engel, S. Pittel, and P. Vogel, *Int. J. Mod. Phys. E* **01**, 1 (1992).
- [23] L. Baudis, G. Kessler, P. Klos, R. F. Lang, J. Menéndez, S. Reichard, and A. Schwenk, *Phys. Rev. D* **88**, 115014 (2013).
- [24] C. McCabe, *J. Cosmol. Astropart. Phys.* **05** (2016) 033.
- [25] J. Fan, M. Reece, and L. T. Wang, *J. Cosmol. Astropart. Phys.* **11** (2010) 042.
- [26] A. L. Fitzpatrick, W. Haxton, E. Katz, N. Lubbers, and Y. Xu, *J. Cosmol. Astropart. Phys.* **02** (2013) 004.
- [27] A. L. Fitzpatrick, W. Haxton, E. Katz, N. Lubbers, and Y. Xu, [arXiv:1211.2818](https://arxiv.org/abs/1211.2818).
- [28] N. Anand, A. L. Fitzpatrick, and W. C. Haxton, *Phys. Rev. C* **89**, 065501 (2014).
- [29] K. Schneck *et al.* (SuperCDMS Collaboration), *Phys. Rev. D* **91**, 092004 (2015).
- [30] E. Epelbaum, H. W. Hammer, and U.-G. Meißner, *Rev. Mod. Phys.* **81**, 1773 (2009).
- [31] R. Machleidt and D. R. Entem, *Phys. Rep.* **503**, 1 (2011).
- [32] H.-W. Hammer, A. Nogga, and A. Schwenk, *Rev. Mod. Phys.* **85**, 197 (2013).
- [33] S. Bacca and S. Pastore, *J. Phys. G* **41**, 123002 (2014).
- [34] G. Prézeau, A. Kurylov, M. Kamionkowski, and P. Vogel, *Phys. Rev. Lett.* **91**, 231301 (2003).
- [35] V. Cirigliano, M. L. Graesser, and G. Ovanessian, *J. High Energy Phys.* **10** (2012) 025.
- [36] J. Menéndez, D. Gazit, and A. Schwenk, *Phys. Rev. D* **86**, 103511 (2012).
- [37] M. Hoferichter, P. Klos, and A. Schwenk, *Phys. Lett. B* **746**, 410 (2015).
- [38] P. Klos, J. Menéndez, D. Gazit, and A. Schwenk, *Phys. Rev. D* **88**, 083516 (2013); **89**, 029901(E) (2014).
- [39] V. Cirigliano, M. L. Graesser, G. Ovanessian, and I. M. Shoemaker, *Phys. Lett. B* **739**, 293 (2014).
- [40] L. Vietze, P. Klos, J. Menéndez, W. C. Haxton, and A. Schwenk, *Phys. Rev. D* **91**, 043520 (2015).
- [41] M. C. Smith *et al.*, *Mon. Not. R. Astron. Soc.* **379**, 755 (2007).
- [42] M. Drees and C. L. Shan, *J. Cosmol. Astropart. Phys.* **06** (2008) 012.
- [43] P. J. Fox, J. Liu, and N. Weiner, *Phys. Rev. D* **83**, 103514 (2011).
- [44] M. Schumann, *EPJ Web Conf.* **96**, 01027 (2015).
- [45] J. D. Lewin and P. F. Smith, *Astropart. Phys.* **6**, 87 (1996).
- [46] R. J. Hill and M. P. Solon, *Phys. Rev. D* **91**, 043505 (2015).
- [47] J. Goodman, M. Ibe, A. Rajaraman, W. Shepherd, T. M. P. Tait, and H. B. Yu, *Phys. Rev. D* **82**, 116010 (2010).
- [48] M. A. Shifman, A. I. Vainshtein, and V. I. Zakharov, *Phys. Lett.* **78B**, 443 (1978).
- [49] A. Kryjevski, *Phys. Rev. D* **70**, 094028 (2004).
- [50] L. Vecchi, [arXiv:1312.5695](https://arxiv.org/abs/1312.5695).
- [51] A. Crivellin, M. Hoferichter, and M. Procura, *Phys. Rev. D* **89**, 054021 (2014).
- [52] M. Hoferichter, J. Ruiz de Elvira, B. Kubis, and U.-G. Meißner, *Phys. Rep.* **625**, 1 (2016).
- [53] V. Baru, C. Hanhart, M. Hoferichter, B. Kubis, A. Nogga, and D. R. Phillips, *Phys. Lett. B* **694**, 473 (2011).
- [54] V. Baru, C. Hanhart, M. Hoferichter, B. Kubis, A. Nogga, and D. R. Phillips, *Nucl. Phys.* **A872**, 69 (2011).
- [55] M. Hoferichter, J. Ruiz de Elvira, B. Kubis, and U.-G. Meißner, *Phys. Rev. Lett.* **115**, 092301 (2015).
- [56] S. Dürr *et al.* (BMW Collaboration), *Phys. Rev. Lett.* **116**, 172001 (2016).
- [57] Y. B. Yang, A. Alexandru, T. Draper, J. Liang, and K. F. Liu (χ QCD Collaboration), [arXiv:1511.09089](https://arxiv.org/abs/1511.09089).
- [58] A. Abdel-Rehim, C. Alexandrou, M. Constantinou, K. Hadjiyiannakou, K. Jansen, Ch. Kallidonis, G. Koutsou, and A. Vaquero Avilés-Casco (ETM Collaboration), *Phys. Rev. Lett.* **116**, 252001 (2016).
- [59] G. S. Bali, S. Collins, D. Richtmann, A. Schäfer, W. Söldner, and A. Sternbeck (RQCD Collaboration), *Phys. Rev. D* **93**, 094504 (2016).
- [60] M. Hoferichter, J. Ruiz de Elvira, B. Kubis, and U.-G. Meißner, *Phys. Lett. B* **760**, 74 (2016).
- [61] P. Junnarkar and A. Walker-Loud, *Phys. Rev. D* **87**, 114510 (2013).
- [62] J. Gasser, H. Leutwyler, and M. E. Sainio, *Phys. Lett. B* **253**, 260 (1991).
- [63] K. A. Olive *et al.* (Particle Data Group Collaboration), *Chin. Phys. C* **38**, 090001 (2014).
- [64] M. Hoferichter, C. Ditsche, B. Kubis, and U.-G. Meißner, *J. High Energy Phys.* **06** (2012) 063.
- [65] C. Ditsche, M. Hoferichter, B. Kubis, and U.-G. Meißner, *J. High Energy Phys.* **06** (2012) 043.
- [66] S. Aoki *et al.*, *Eur. Phys. J. C* **74**, 2890 (2014).
- [67] P. G. Ratcliffe, *Phys. Lett. B* **365**, 383 (1996).
- [68] T. Yamanishi, *Phys. Rev. D* **76**, 014006 (2007).
- [69] T. R. Hemmert, U.-G. Meißner, and S. Steininger, *Phys. Lett. B* **437**, 184 (1998).
- [70] H.-W. Hammer, S. J. Puglia, M. J. Ramsey-Musolf, and S. L. Zhu, *Phys. Lett. B* **562**, 208 (2003).
- [71] B. Kubis and R. Lewis, *Phys. Rev. C* **74**, 015204 (2006).
- [72] A. Antognini *et al.*, *Science* **339**, 417 (2013).
- [73] R. González-Jiménez, J. A. Caballero, and T. W. Donnelly, *Phys. Rev. D* **90**, 033002 (2014).
- [74] A. Airapetian *et al.* (HERMES Collaboration), *Phys. Rev. D* **75**, 012007 (2007).
- [75] V. Bernard, L. Elouadrhiri, and U.-G. Meißner, *J. Phys. G* **28**, R1 (2002).
- [76] M. R. Schindler, T. Fuchs, J. Gegelia, and S. Scherer, *Phys. Rev. C* **75**, 025202 (2007).
- [77] S. Weinberg, *Phys. Lett. B* **251**, 288 (1990).
- [78] S. Weinberg, *Nucl. Phys.* **B363**, 3 (1991).
- [79] D. B. Kaplan, M. J. Savage, and M. B. Wise, *Phys. Lett. B* **424**, 390 (1998).
- [80] D. B. Kaplan, M. J. Savage, and M. B. Wise, *Nucl. Phys.* **B534**, 329 (1998).
- [81] M. Pavón Valderrama and D. R. Phillips, *Phys. Rev. Lett.* **114**, 082502 (2015).

- [82] S. R. Beane, S. D. Cohen, W. Detmold, H.-W. Lin, and M. J. Savage, *Phys. Rev. D* **89**, 074505 (2014).
- [83] E. Caurier, J. Menéndez, F. Nowacki, and A. Poves, *Phys. Rev. Lett.* **100**, 052503 (2008).
- [84] J. Menéndez, A. Poves, E. Caurier, and F. Nowacki, *Nucl. Phys.* **A818**, 139 (2009).
- [85] E. Caurier and F. Nowacki (1999), <http://www.actaphys.uj.edu.pl/fulltext?series=Reg&vol=30&page=705>.
- [86] E. Caurier, G. Martínez-Pinedo, F. Nowacki, A. Poves, and A. P. Zuker, *Rev. Mod. Phys.* **77**, 427 (2005).
- [87] E. Epelbaum, H. Krebs, and U.-G. Meißner, *Eur. Phys. J. A* **51**, 53 (2015).
- [88] R. J. Furnstahl, N. Klco, D. R. Phillips, and S. Wesolowski, *Phys. Rev. C* **92**, 024005 (2015).
- [89] B. D. Carlsson, A. Ekström, C. Forssén, D. F. Strömberg, G. R. Jansen, O. Lilja, M. Lindby, B. A. Mattsson, and K. A. Wendt, *Phys. Rev. X* **6**, 011019 (2016).
- [90] J. Simonis, K. Hebeler, J. D. Holt, J. Menéndez, and A. Schwenk, *Phys. Rev. C* **93**, 011302 (2016).
- [91] T. W. Donnelly and W. C. Haxton, *At. Data Nucl. Data Tables* **23**, 103 (1979).
- [92] W. Haxton and C. Lunardini, *Comput. Phys. Commun.* **179**, 345 (2008).
- [93] V. Cirigliano and M. L. Graesser (private communication).
- [94] J. Menéndez, D. Gazit, and A. Schwenk, *Phys. Rev. Lett.* **107**, 062501 (2011).
- [95] J. Engel, F. Šimkovic, and P. Vogel, *Phys. Rev. C* **89**, 064308 (2014).
- [96] W. N. Cottingham, *Ann. Phys.* **25**, 424 (1963).
- [97] J. Gasser and H. Leutwyler, *Nucl. Phys.* **B94**, 269 (1975).
- [98] J. Gasser, M. Hoferichter, H. Leutwyler, and A. Rusetsky, *Eur. Phys. J. C* **75**, 375 (2015).
- [99] S. Borsanyi *et al.*, *Science* **347**, 1452 (2015).
- [100] A. Crivellin, M. Hoferichter, M. Procura, and L. C. Tunstall, *J. High Energy Phys.* 07 (2015) 129.
- [101] R. J. Hill and M. P. Solon, *Phys. Rev. D* **91**, 043504 (2015).
- [102] A. Crivellin, F. D’Eramo, and M. Procura, *Phys. Rev. Lett.* **112**, 191304 (2014).
- [103] A. Crivellin and U. Haisch, *Phys. Rev. D* **90**, 115011 (2014).
- [104] F. D’Eramo and M. Procura, *J. High Energy Phys.* 04 (2015) 054.